energies

MDPI

Review

Electrochemical Failure Results Inevitable Capacity Degradation in Li-Ion Batteries—A Review

Wei Li [1], Hang Li [1], Zheng He [2], Weijie Ji [1], Jing Zeng [1], Xue Li [3], Yiyong Zhang [3], Peng Zhang [2,*] and Jinbao Zhao [1,*]

[1] State-Province Joint Engineering Laboratory of Power Source Technology for New Energy Vehicle, State Key Laboratory of Physical Chemistry of Solid Surfaces, Engineering Research Center of Electrochemical Technology, Collaborative Innovation Center of Chemistry for Energy Materials, College of Chemistry and Chemical Engineering, Ministry of Education, Xiamen University, Xiamen 361005, China
[2] College of Energy & School of Energy Research, Xiamen University, Xiamen 361102, China
[3] National and Local Joint Engineering Laboratory for Lithium-Ion Batteries and Materials Preparation Technology, Faculty of Metallurgical and Energy Engineering, Kunming University of Science and Technology, Kunming 650093, China
* Correspondence: pengzhang@xmu.edu.cn (P.Z.); jbzhao@xmu.edu.cn (J.Z.)

Abstract: Lithium-ion batteries (LIBs) have been widely used in mobile devices, energy storage power stations, medical equipment, and other fields, became an indispensable technological product in modern society. However, the capacity degradation of LIBs limits their long-term deployment, which is not conducive to saving resources. What is more, it will lead to safety problems when the capacity of the battery is degraded. Failure of the battery is a key issue in the research and application of LIBs. Faced with the problem of capacity degradation, various aspects of LIBs have been studied. This paper reviews the electrochemical degradation mechanism of LIBs' life fade, detection technologies for battery failure, methods to regulate battery capacity degradation, and battery lifetime prognostics. Finally, the development trend and potential challenges of battery capacity degradation research are prospected. All the key insights from this review are expected to advance the research on capacity fading and lifetime prediction techniques for LIBs.

Keywords: failure; capacity degradation; battery failure detection; battery lifetime prognostics

Citation: Li, W.; Li, H.; He, Z.; Ji, W.; Zeng, J.; Li, X.; Zhang, Y.; Zhang, P.; Zhao, J. Electrochemical Failure Results Inevitable Capacity Degradation in Li-Ion Batteries—A Review. *Energies* **2022**, *15*, 9165. https://doi.org/10.3390/en15239165

Academic Editor: Jun Young Cheong

Received: 31 October 2022
Accepted: 28 November 2022
Published: 2 December 2022

1. Introduction

The large use of non-renewable resources, such as oil, coal, and natural gas, brings the potential greenhouse effect, and exacerbates global climate change. In recent years, renewable energy such as wind and solar are considered major components to build a sustainable society. Whereas, sustainable society realization depends on the efficiency and sustainability of energy storage technologies [1]. Energy storage technology can store intermittent renewable energy and further penetrate into the power system to achieve a continuous energy supply [2]. Thus, energy storage technology is more important today than ever before. As a type of mobile energy storage device, LIBs are considered to be a kind of clean energy carrier with high energy density, long cycle life, no pollution, and no memory effect [3]. What is more, they are expected to be widely used in stationary energy storage, smart grid, electric transportation, new technology equipment, and other applications [4,5]. In recent years, LIBs have made great progress in increasing energy density, reducing cost, and fast charging. Advances in battery technology also have driven the development of electric vehicles (EVs). With the continuous improvement of LIBs, EVs are gradually replacing fuel vehicles, which save non-renewable resources and slow down the environmental pollution problem [6–8]. However, LIBs still face major problems, the most important challenge is the inevitable capacity degradation of LIBs in operation [9–11].

The ideal charging and discharging process of LIBs is a reversible electrochemical reaction. However, the polarization of the electrochemical reaction and the damage of the active material during long-term usage will destroy the reversibility of the electrochemical reaction, which leads to the capacity degradation of the battery.

The degradation of LIBs capacity makes it a great influence in long-term application, resource saving, and battery safety [12–14]. The use of batteries in extreme conditions, for example, fast charging and low-temperature cycling, has a greater impact on the life decay of LIBs. Especially, the EVs pursue a high driving time/charging time ratio. In this case, the capacity degradation problem is more serious [15]. So, the capacity degradation of power batteries is the primary problem that must be solved. To achieve the purpose of reducing capacity decay, it is very important to explore the failure mechanism and predict the degradation of LIBs [16].

The degradation of battery capacity is complicated by the operation, which is caused by multiple factors. Unfortunately, these factors do not work independently, but interact and couple tightly [17]. There are many factors including collapse and micro cracks of the cathode material, the expansion and pulverization of the anode material [18], the thickening of the solid-electrolyte interphase (SEI), the inevitable formation of lithium plating, and the corrosion of the current collector. What is worse is that these problems interact together to affect the battery performance and capacity. For example, the thickening of SEI will aggravate the possibility of lithium plating. Changes in the structure and decomposition of these battery materials may even cause a decrease in the safety performance of the battery [19,20]. Identifying the aging mechanism in LIBs is the main challenging goal [21]. Therefore, studying the influence of these factors on battery life is the necessary way to prevent battery failure, slow down the speed of life decay, and establish a life prediction model [13,22].

This review describes the mechanism for the capacity degradation of LIBs from the electrochemical reaction of active material. Based on the performance of battery fading, it lists characterization methods including destructive detection and non-destructive detection. According to the failure mechanism, a variety of improvement methods for attenuating capacity degradation are proposed. Finally, the battery life prediction methods are described to achieve better control in EVs.

2. Battery Failure Mechanism

Failure of Cathode Material

The lithium that provides reversible electrochemical behavior in the battery only comes from the cathode. In addition, the capacity of the anode is higher than that of the cathode when the battery is designed, so the capacity of the cathode determines the capacity of the entire battery. The capacity of the cathode is considered to be the main limiting factor for the further improvement of the energy of the LIBs [23]. Cathode materials that have been commercialized at present mainly include $LiMn_2O_4$ (LMO), $LiFePO_4$ (LFP), $LiCoO_2$ (LCO), $Li[Ni_xCo_yMn_z]O_2$ (NCM), and so on (Table 1).

Table 1. Related parameters of common cathode materials.

Cathode Materials	Theoretical Capacity ($mAh \cdot g^{-1}$)	Potential (V vs. Li/Li^+)	Crystal Structure
LMO	148	3.0–4.3	Spinel structure
LFP	170	3.2–3.7	Olivine structure
LCO	274	3.0–4.5	layered structure
NCM	273–285	2.5–4.6	layered structure
NCA	279	3.0–4.2	layered structure
V_2O_5	294	2.0–4.0	layered structure

As the earliest commercial cathode material for LIBs, LCO has the advantages of excellent volumetric energy density, high theoretical capacity, and excellent rate performance [24,25]. It still plays an important role in the LIBs market. At present, the main research on LCO is to improve the charge cut-off voltage, and make it play at a higher capacity. However, with the increase in charging voltage, a series of side reactions will occur, such as irreversible transformation from O3 phase to H1-3 phase transition, deterioration of positive electrode interface, dissolution of cobalt element, and precipitation of lattice oxygen, resulting in increased internal resistance and rapid deterioration of battery performance, which greatly limits the practical application of high-voltage lithium cobalt [26]. LFP is another cathode material that has been used on a large scale. As a result of the advantages of an extended cycle life, excellent thermal stability, and high specific capacity. In the LFP structure, the PO_4 tetrahedron locates between the LiO_6 octahedron and FeO_6 octahedron, with only narrow one-dimensional "holes" formed for lithium ions diffusion, which limits the insertion and extraction of Li in charging and discharging processes. Furthermore, the lack of a continuous FeO_6 octahedral network confines the electrons in the Fe-O-Fe path during conduction, leading to a poor electronic conductivity of LFP [27–29]. Therefore, improving material conductivity is the main direction of LFP cathode research.

The actual use capacity of NCM cathode has reached 160–220 mAh g^{-1}, so NCM cathode materials have been widely used in the field of EVs [30]. In the NCM material, nickel is the main element of the redox reaction; therefore, increasing the content of nickel can improve the specific capacity of the material, and the Ni-rich ternary material has become an important development direction. However, Ni-rich materials are prone to problems such as cation mixing, cracking, and structural collapse during cycling [31]. At the same time, with the increase in nickel content, the alkalinity of the material's surface increases; therefore, it is more sensitive to air and carbon dioxide, which requires stricter requirements for the storage of materials and the production of electrodes [32]. In this section, we will summarize the failure modes and mechanisms from the bulk and surface of cathode materials. Layered transition metal (TM) oxides have a regular layered α-$NaFeO_2$ type crystal structure. In this structure, TM and Li^+ alternately occupy octahedral sites in a cubic close-packed oxygen lattice [33]. It will cause the material structure from layered change to defect spinel or disordered rock-salt [34–36]. Lin et al. [37] explored the structural and chemical evolution of the layered $Li[Ni_{0.8}Co_{0.1}Mn_{0.1}]O_2$ (NCM811) at the atomic scale in detail. They found the structure of cathode materials changes gradually from a well-layered in the bulk to disordered layered, defective rock-salt, and eventually rock-salt phase near the surface in which the Li diffusion paths have been entirely blocked by TM cations (Figure 1a–c). The rock-salt phase of the cathode material is more advantageous at higher voltages, and the highly oxidative environment triggers the loss of oxygen in the material. The ionically insulating rock-salt phase may lead to kinetic sluggishness and thus deteriorated capacity retention [38]. JooNoh et al. [39] studied the electrochemical properties and thermal stability of Ni-rich materials and obtained a function of Ni content with electrochemical properties and thermal stability (Figure 1d–i). With the increasing Ni content, the particle size significantly decreases which will lead to an increase in the contact area between the material and electrolyte. Whereas, the increase in Ni content leads to a rapid decrease in thermal stability so that the advantage gained by the increased discharge capacity is quickly negated by the deterioration of the battery safety (Figure 1j–k). Moreover, due to the anisotropy inside the secondary particles, the expansion and contraction of crystals occurring during the charging and discharging cycle will gradually form microcracks, which will result in parasitic reactions [40,41]. It has to be clear that NCM materials will be simultaneously subjected to the above-mentioned reactions during the life cycle. From the above content, it can be seen that the synthesis of more stable cathode materials by modification is an effective method to alleviate material failure.

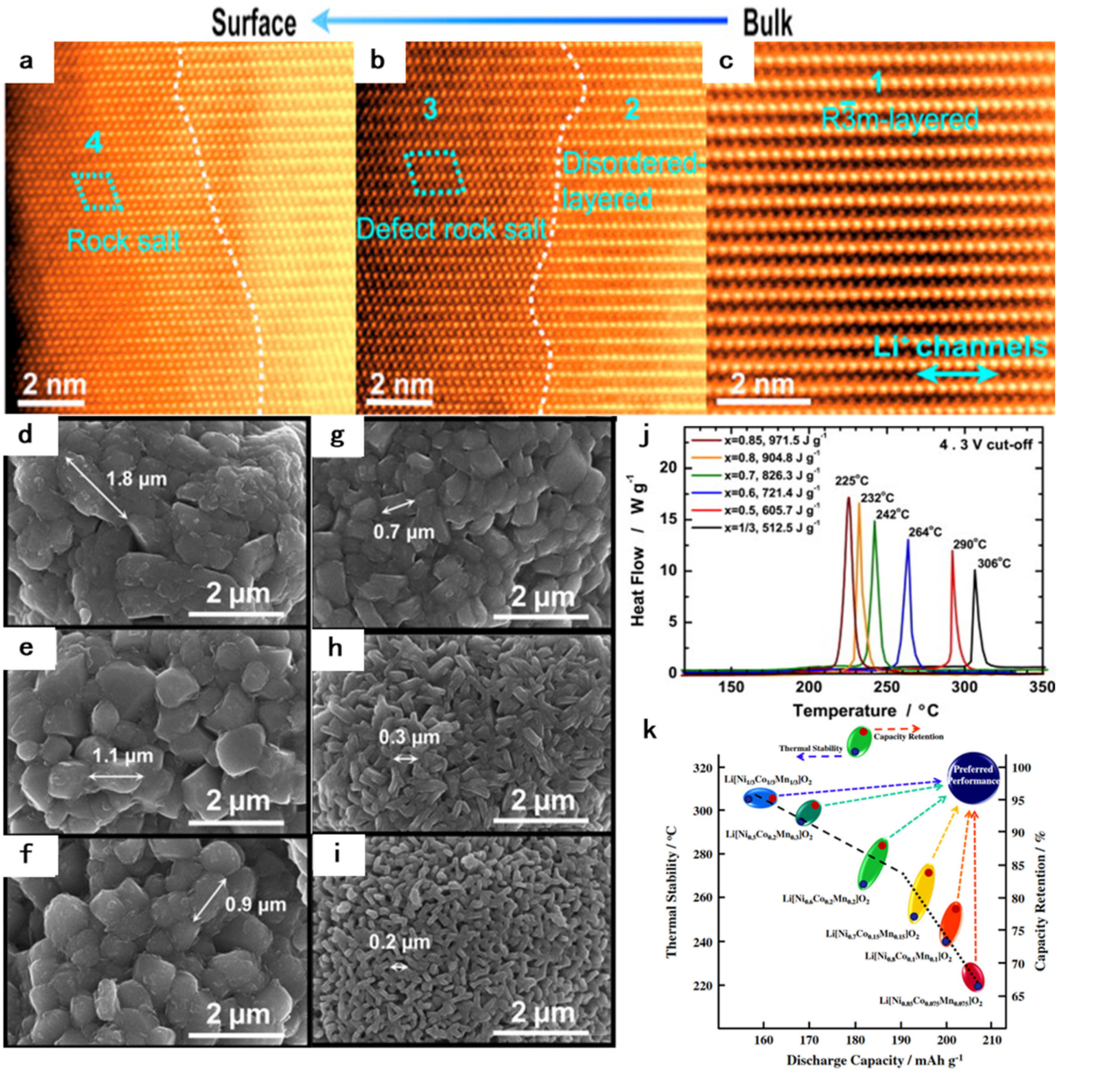

Figure 1. (**a**–**c**) Atomic-resolution STEM-HAADF and ABF images captured on NMC811 cathode after 100 cycles with cut-off voltage of 4.5 V in <010> zone projection. The STEM-HAADF images at different regions from bulk to surface. The white dashed lines denote the surface reconstruction layer at different stages; Reprinted with permission from Ref. [37]. 2018, Elsevier. (**d**–**i**) SEM images of the $Li[Ni_xCo_yMn_z]O_2$ powders: (**d**) x = 1/3, (**e**) x = 0.5, (**f**) x = 0.6, (**g**) x = 0.7, (**h**) x = 0.8 and (**i**) x = 0.85; (**j**) DSC results of the $Li[Ni_xCo_yMn_z]O_2$ materials (x = 1/3, 0.5, 0.6, 0.7, 0.8, and 0.85). (**k**) A map of relationship between discharge capacity, and thermal stability and capacity retention of $Li/Li[Ni_xCo_yMn_z]O_2$ (x = 1/3, 0.5, 0.6, 0.7, 0.8, and 0.85). Reprinted with permission from Ref. [39]. 2013, Elsevier.

What is more, the safety problems caused by the failure of cathode materials should not be underestimated, especially thermal runaways that occurred in ternary materials batteries. Low thermal stability is typically caused by detrimental oxygen release from the cathode, which will lead to significant safety concerns [42]. Hou et al. [43] revealed the thermal runaway mechanisms of LIBs with the NMC811 cathode. They considered

the cathode-generated oxygen to be the core process of the thermal runaway. Approximately 41% of thermal-induced O_2/O* reacts violently with ethylene carbonate (EC) at the cathode/electrolyte interface with 16% heat generation. This part of heat accelerates the self-heating of LIBs, which further triggers thermal runaway. What is more serious is that the remaining O_2/O* spreads to the anode, they react with the lithiated anode and generate a lot of heat (65%), making the LIBs to the highest temperature during thermal runaway. (Figure 2a–c). It can be seen that the failure of cathode materials brings not only the degradation of battery capacity but also the safety problem. Therefore, more attention should be paid to the failure study of cathode materials, and the reliability of cathode materials should be improved from the perspective of materials.

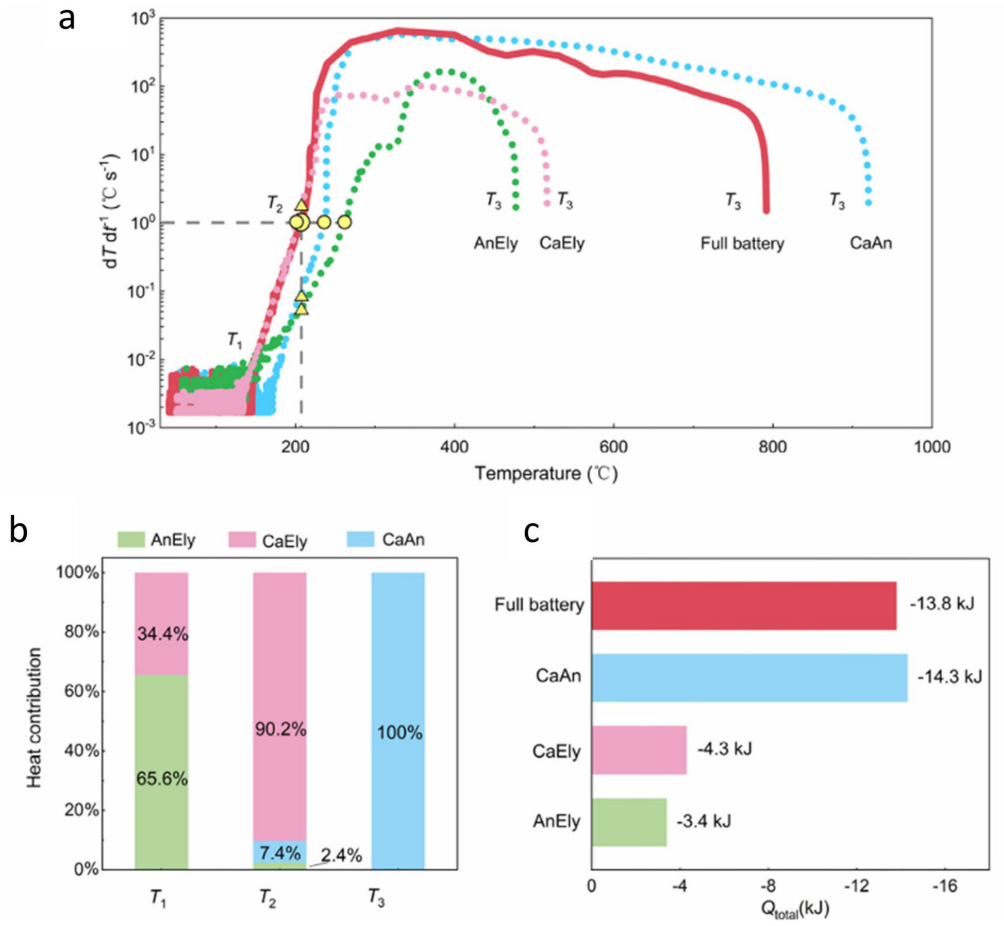

Figure 2. Reaction heat of fully charged NMC811 | Gr pouch cell and partial cells during thermal runaway. Reproduced with permission Reprinted with permission from Ref. [43]. 2021, Elsevier. (**a**) Temperature dependence of dT dt^{-1} (dT dt^{-1} vs. T) for full battery and partial cells, where the characteristic temperatures of T_1, T_2, and T_3 are marked and compared.; (**b**) Proportion of heat generation of partial cells to the full battery at T_1, T_2, and T_3.; (**c**) Heat generation (Qtotal) of the full battery and partial cells during thermal runaway.

3. Anode Materials and Their Interface Failure Problems

Cathode material is an effective carrier of reversible lithium in LIBs. The electrochemical performance of the anode has a profound impact on the Coulombic efficiency and the cycle life of the battery. Although the specific capacity of the anode material (330 mAh g^{-1}) is higher than that of the cathode material (150–200 mAh g^{-1}), it is still expected to find an anode material with a higher specific capacity to improve the bulk energy density of the power battery. However, this kind of anode material faces a more serious failure phenomenon in

the actual use process. According to the current application and research status, the anode materials of LIBs and their basic properties can be listed in Table 2.

Table 2. Anode materials of LIBs and their basic properties.

Anode Materials	Theoretical Capacity ($mAh \cdot g^{-1}$)	Potential (V vs Li/Li^+)	Volume Expansion Rate (%)
Graphite	372	0.01–0.2	12
$Li_4Ti_5O_{12}$	175	1.4–1.6	1
Si	4200	0.2	300
Sn	994	0.6–0.1	260

Graphite has dominated LIBs anode materials since the birth of LIBs because of the abundant reserves and excellent cycle performance, especially the considerable specific capacity and low de-lithiation potential [44,45], Graphite is the layer structure material which can store lithium through the intercalation/de-intercalation reaction, which Li-ions can reversibly intercalate and de-intercalate into the lattice of layer materials without destroying the crystal structure [46]. During the initial lithiation of the graphite electrode, The electrolyte solvents and salts will decompose on the graphite surface and form a thin layer known as the solid electrolyte interphase (SEI) on the surface [47]. The ideal SEI as a passivation layer can prevent further interfacial reaction of electrolytes. However, the formation of SEI consumes reversible Li-ions from the cathode, which leads to an irreversible active materials loss. In addition, graphite will expand by 12% in volume after intercalated, which can easily lead to the rupture of SEI. The graphite contacts the electrolyte again and forms a new SEI during the charging process. The ever-thickening SEI will lead to the loss of active lithium and an increase in the internal resistance, making the battery capacity drop rapidly [48,49]. What is worth studying is to establish a reliable and stable SEI, which can better promote the electrochemical performance of the anode and delay the degradation of battery capacity.

What is more, it is worth noting that the unit mass capacity of graphite (372 mAh g^{-1}) is still not enough. Yoshio et al. [50] found that increasing the capacity of the anode material has a very large contribution to the mass energy density of the battery in the range of 300–1200 mAh g^{-1}. Pursued for their higher mass-specific capacity, silicon-based anodes have become the focus of LIBs research, and it is very promising to be applied in commercial LIBs anode material [20]. Unlike graphite which relies on intercalation, the mechanism of lithium storage in the silicon anode is the reaction of silicon particles with lithium to form lithiated silicide structures, which have a mass special capacity of 4200 mAh g^{-1}. However, the repeated lithiation/de-lithiation reaction during the charging and discharging process leads to the breaking/recombination of Si-Si bonds, which can cause the change of the Si particles, More seriously is lithiated silicide volume expanded to 300%, when the battery is fully charged [51], and huge volume change can lead to the pulverization of silicon particles, loss of electrical contact, and SEI rupture [52–55]. Using scanning transmission microscopy, Wetjen et al. [56] observed the morphology of silicon anodes with a different number of cycles (Figure 3a). Before the charge and discharge cycle, the silicon particles showed an irregular shape, consisting of a dense crystal structure. After the first cycle, the shape and size of the silicon were still very similar, while the silicon surfaces tended to be less smooth and the edges less sharp. What is more, it could be noticed that the change in silicon particle morphology became less and less significant as the number of cycles increases. He et al. [20] found that the gradual growth of solid electrolytes into silicon anode leads to capacity degradation, and revealed the related structure and chemical evolution of Si and SEI in three-dimensional space (Figure 3b–e). Through transmission electron microscopy (TEM), McDowell et al. [57] observed the time-varying lithiation and fracture of large nanoparticles (initial diameter ~450 nm), (Figure 3f–n). The speed of lithiation of large particles was lower than that of small particles, and the large particles were prone to

fracture and become electrically isolated during the process of lithiation. The huge volume expansion of the silicon anode and the inward penetration of SEI accelerate the failure of the anode and hinder the further development of the silicon anode.

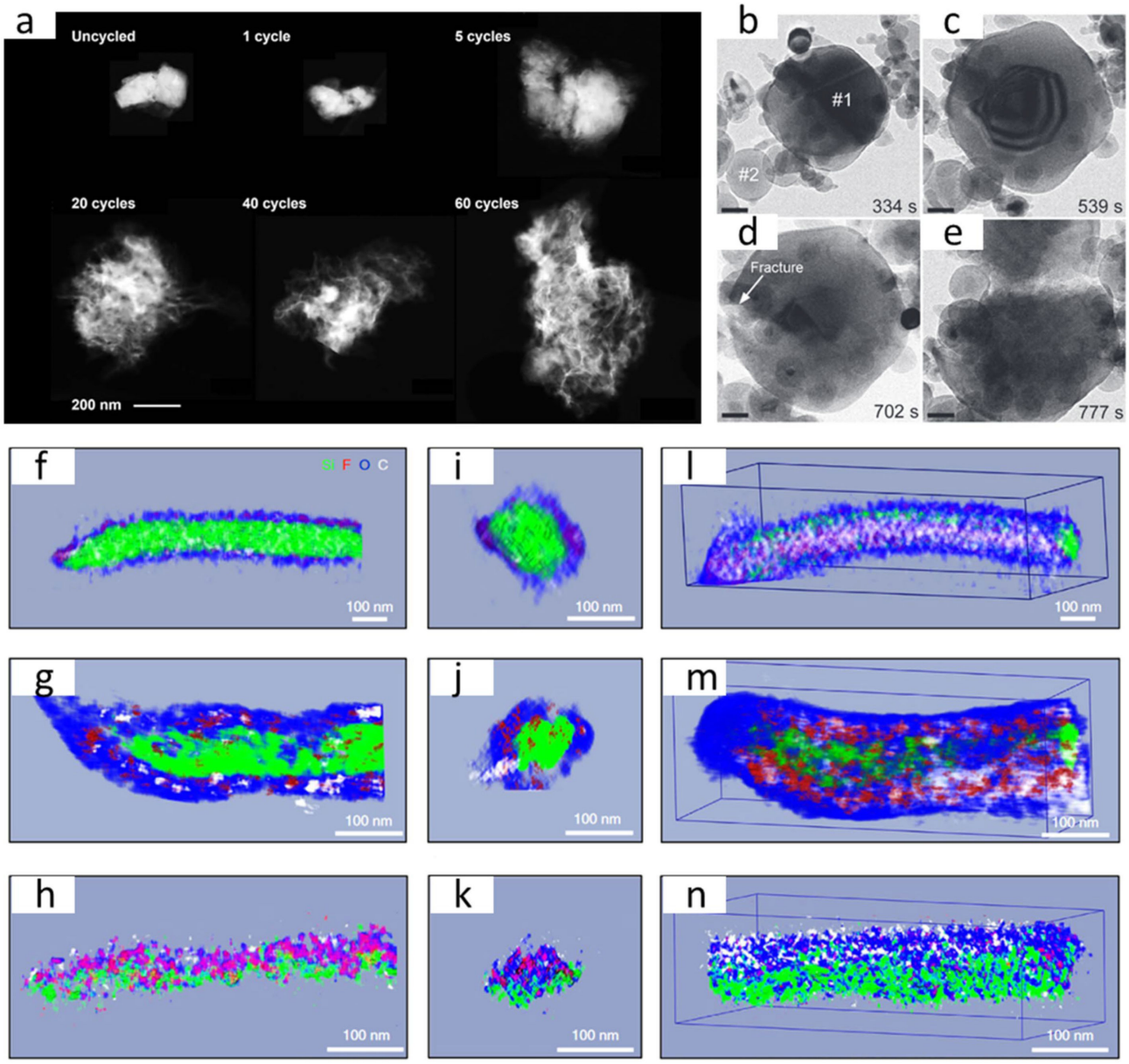

Figure 3. (**a**) Scanning transmission microscope image of silicon particles cycling with different number of cycles Reprinted with permission from Ref. [56]. 2018, Iopscience. (**b**–**e**) Time-series of images of the lithiation and fracture of a large (∼450 nm initial diameter) nanoparticle. The lithiated lithium source is to the left of the frame. (**b**) Lithiation has just started to occur, with the Li_xSi phase visible around the edges of particle #1. Particle #2 has already become partially lithiated. (**c**) The crystalline Si core is clearly visible as the darker-contrast region in the center of particle #1. (**d**) Fracture initiates at the left surface of particle #1. (**e**) After fracture, the interior Si region of the particle is quickly lithiated and the crack grows, tearing the particle apart. Reprinted with permission from Ref. [20]. 2012, Wiley. (**f**–**n**) Segmented viewing of 3D cryo-STEM-EDS chemical composition from two directions, Segmented view parallel to the wire axis after the 1st cycle (**f**), 36th cycle (**g**), and 100th cycle (**h**). Slice thickness is 5 nm. Segmented cross-section view for the 1st (**i**), 36th (**j**), and 100th (**k**) cycles. The 3D view for the 1st (**l**), 36th (**m**), and 100th (**n**) cycles. Reprinted with permission from Ref. [57]. 2018, Nature.

The market share of $Li_4Ti_5O_{12}$ (LTO) in the field of LIBs anode materials is second only to graphite [58]. Excellent cycle stability, rate capability, and thermal stability are its biggest advantages. Of course, there are also low capacity and gassing issues and other disadvantages [59–61]. The gases generated by LTO during the cycle and storage process mainly contain H_2, CO_2, and CO. These gases come from the interfacial reaction between LTO and the alkyl carbonate solvents. Serious expansion will lead to safety problems [62]. In addition, Sn-based anode is another promising material with high theoretical capacity, but its commercialization is limited by the dramatic volume changes during lithium insertion/extraction [63]. The volume change brings about a series of problems, including pulverization of active particles, continuous breaking and regeneration of SEI, thus consuming lithium sources, etc. [64,65].

To sum up, the traditional mature graphite anode has the limitation of specific capacity and fast charging performance, while the silicon and Sn-based anode with very high specific capacity has the volume expansion problem and other problems that may be found in future research. What is more, the capacity of LTO is low and there is a flatulence problem. At the same time, the construction of SEI also plays a non-negligible role in battery cycle and battery safety. Therefore, research on these aspects will be a focus of future work.

4. Lithium Plating

In the current field of LIBs, graphite has an unshakable position in the anode material. The mechanism of graphite intercalation is intercalate/de-intercalate, and because the potential of lithium intercalation into graphite is in the range of 0.2 to 0.065 V vs. Li/Li^+, when the sum of the equilibrium potential and the overpotential becomes negative vs. Li/Li^+, the lithium deposition on the graphite will happen, and this phenomenon called Li-plating [46,66]. Li-plating not only is a predominant cause for capacity decay during the fast charging of LIBs but also brings hidden danger for the thermal runaway of the battery. Moreover, because lithium metals tend to form as lithium dendrites, the dendrites are likely to pierce the separator, causing a short circuit in the LIBs, even leading to thermal runaway [66–68]. Therefore, we must understand the mechanism of Li-plating and detect the amount of Li-plating in real time. According to past research, the phenomenon of Li-plating occurrence depends not only on charging speed but also on temperature during the cycle and electrode design [66,69–71]. In this section, we will carefully analyze the factors that lead to the occurrence of lithium plating.

Li et al. [71] researched the effect of the areal capacity ratios of negative to positive electrodes (N/P ratio), they circulated the LIBs for 5 cycles in the voltage range of 2.75–4.2 V at a rate of 3 C at room temperature. The LIBs after circulation are disassembled, and Li-plating on the anode surface can be observed by SEM. They found that Li-plating becomes less with increasing N/P ratio (Figure 4a–f). A too-high N/P ratio will lead to excessive SEI and consume a lot of active substances, while a low N/P ratio will lead to Li-plating. Therefore, choosing an appropriate N/P ratio is key to optimizing battery design and improving battery cycle capacity. In addition, whether in the field of EVs or electronic products, fast charging has become an important goal to pursue. However, at high charging currents, the separator and anode interface experience large ion fluxes, which can easily lead to Li-plating, reducing capacity and causing safety problems [72,73]. Ren et al. [12] chose four aging paths of high-temperature storage, low-temperature cycling, high-temperature cycling, and fast charging at room temperature for experiments, and studied the anode of LIBs after cycling, and found that SEI growth results in the loss of recyclable lithium. At the same time, the intercalation of Li-ions in the graphite particles and the Li-plating on the particle surface are competing. The high charge current or low temperature causes slow migration resulting in limited charge transfer at the particle/SEI interface. Lithium electroplating occurs when the graphite potential drops below 0 V relative to Li/Li [74]. What should be paid more attention to is that Li-plating will not only bring the attenuation of battery capacity, but more serious is that the more Li-plating, the more heat the battery generates, and the more prone to thermal runaway. Li et al. [75]

obtained the same conclusion by cycling the battery at different rates to obtain the battery with different amounts of Li-plating and then carried out the thermal experiment of absolute heat (Figure 4g,h) it is obvious that the self-generated heat temperature (T_1) and the trigger temperature of thermal runaway (T_2) will be much lower for batteries with more Li-plating quantity. Li-plating is a serious problem in LIBs, and various strategies to reduce Li-plating are also a research hotspot.

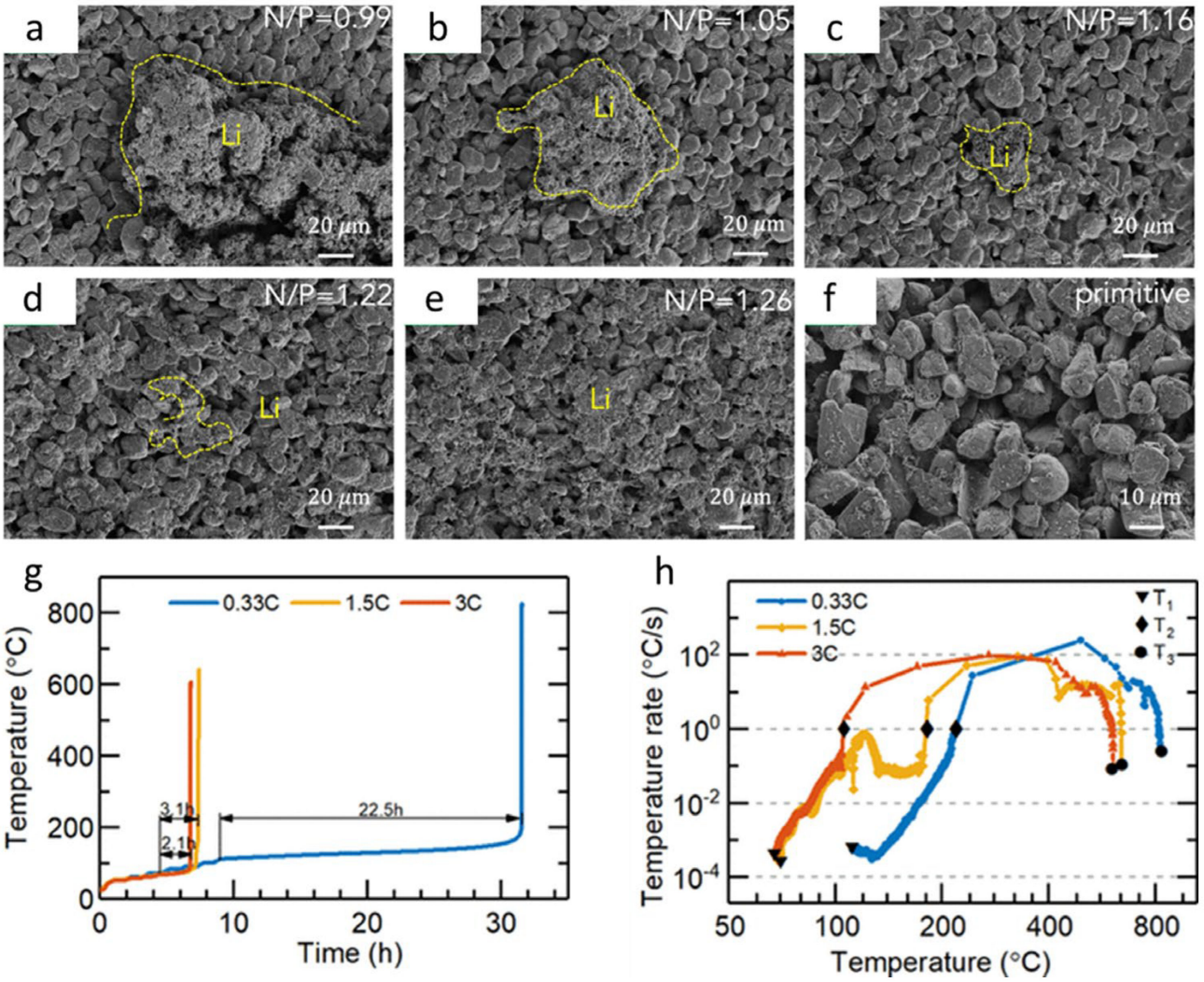

Figure 4. (**a**–**f**) Images showing the graphite SEM of different N/P battery; Reprinted with permission from Ref. [71]. 2018, Elsevier. (**g**,**h**) accelerated rate calorimetry (ARC) tests the thermal runaway behavior of batteries at different charging rates (0.33 C, 1.5 C, and 3 C). Reprinted with permission from Ref. [75]. 2019, ACS Publications.

5. Battery Failure Detection

With the aging cycle of LIBs, the occurrence of battery deterioration cannot be avoided. The detection of battery deterioration is expected to extract important deterioration identification eigenvalues. On the one hand, these eigenvalues are the most important theoretical basis for us to study the deterioration mechanism, promote material research and development and cell design; on the other hand, learning the deterioration eigenvalues can achieve early identification of battery deterioration and prevent the harm caused by battery deterioration. In this review, failure detection is divided into two parts: destructive detection and non-destructive detection. Destructive detection can go deeper into the mechanism, and non-destructive detection can analyze the battery without damage.

6. Destructive Detection

Destructive detection may be the most direct method for revealing the mechanism of the battery failure. This method archive disassembles a large number of batteries with different lifetimes and uses different characterization methods for analysis. Common battery material characterization tests include X-ray diffraction (XRD), scanning electron microscopy (SEM), inductively coupled plasma atomic emission spectroscopy (ICP-AES), high-resolution transmission electron microscopy (HR-TEM), and so on. Accurate, comprehensive, and in-depth analysis of battery materials will produce a more accurate failure mechanism.

First, the loss of active lithium is an important factor causing capacity fading; therefore, detecting the loss of active lithium is an important part of failure detection. Sreenarayanan et al. [76] quantified Li-Si and SEI in Si anode using titration gas chromatography (TGC) in both half-cell and full-cell systems. In order to determine the relative amount of dead lithium produced during the battery cycle, Li et al. [77] weighed the anode surface material and used it for the TGC experiment to characterize the SEI and dead lithium composition on the surface of the lithium metal electrode; that is, the loss amount of active lithium. In addition to the loss of active materials, the failure of the cathode material also has a great impact on the battery performance. For the deterioration of cathode material, Kong et al. [78] tested the section of the cathode material after dismantling the full-charge battery through SEM. It can be seen that the inner part of the single-crystal (SC) material is relatively regular and there is no obvious crack, while for the polycrystalline (PC) material, due to the existence of a crystal gap, obvious shrinkage occurs during the charging process, leading to the formation of holes. (Figure 5b−e). In addition, the effect of different charge and discharge rates on battery failure is undoubtedly inconsistent. For the failure study of different cycle rates, Zhang et al. [79] displayed the distribution of the thickness of the deposited layer and surface morphology of the material at 1 C, 2 C, and 3 C charging C-rates by SEM of anode/cathode (Figure 5f). It is easy to find that more Li-plating occurs on the surface of the anode material as the magnification increases and the structural collapse of the cathode material is more obvious. In addition to material structural changes, composition analysis of the material surface of LIBs is also very necessary in failure analysis. XPS is an important technology to identify the deterioration mechanism, which is often used to detect the composition of the material surface. Yang et al. [80] designed asymmetric temperature modulation for extremely fast charging of LIBs, and high-resolution XPS tests were further carried out to study the SEI structure of the battery at different charging temperatures, XPS spectra showed higher concentrations of C, F, and P and lower concentrations of O and Li in the 60 °C cell compared to the 26 °C cell (Figure 5g,h). Contrary to conventional wisdom, their proposed study significantly improved the life cycle with increasing charge temperature, which will mitigate Li-plating at elevated temperatures. Through various means, we can go deep into the material level, deeply analyze the mechanism of battery failure, and provide guidance for battery design and material modification.

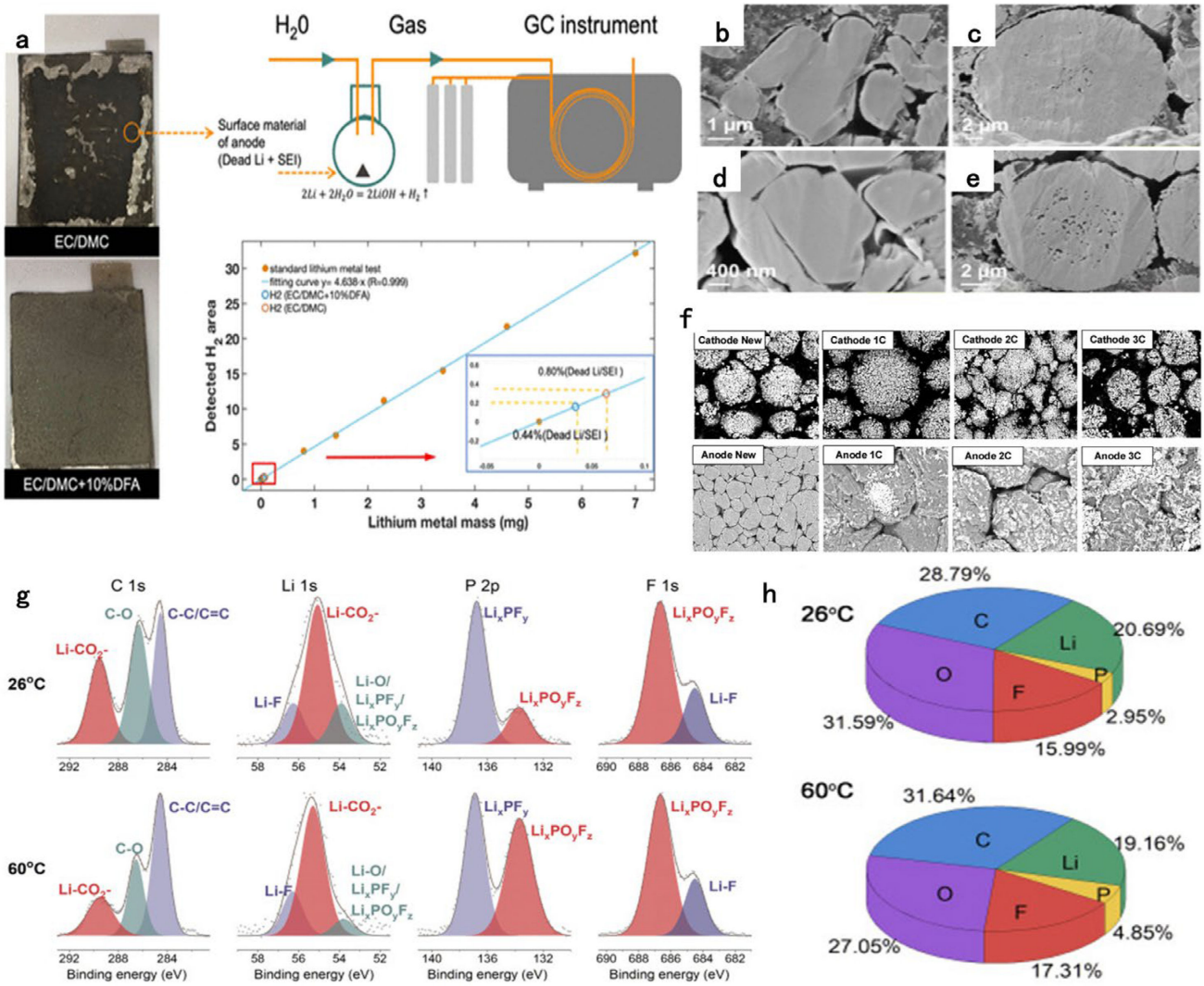

Figure 5. (**a**) Schematic diagram of TGC detection. Reprinted with permission from Ref. [76]. 2021, ACS Publications; (**b**–**e**) SEM test results of the cross-sections tests of four materials at 4.3 V; (**b**) SC-NCM622, (**c**) PC-NCM622, (**d**) SC-NCM811, (**e**) PC-NCM811. Reprinted with permission from Ref. [77] 2022, Elsevier; (**f**) the deposited layer and surface morphology of the cathode/anode material at 1C, 2C, and 3C charging C-rates by SEM. Reprinted with permission from Ref. [79]. 2020, Elsevier; (**g**) high-resolution XPS spectra of C 1s, Li 1s, P 2p, and F 1s of the anode samples from the 26 °C and 60 °C cells; (**h**) elemental concentration of the anode samples from the 26 °C and 60 °C cells. Reproduced with permission. Reprinted with permission from Ref. [80]. 2019, Elsevier.

7. Nondestructive Detection

Destructive detection can provide clear and visual evidence of battery deterioration, but this damage is irreversible for the battery. It is believed that the battery cannot be recovered after destructive detection. This is not a quick and direct method for the deterioration detection of power batteries. Besides, the cost of such methods is too high in the actual use process or research, but non-destructive testing can infer the failures in the battery through the measurable data of batteries or some advanced equipment. This method is economical, fast, harmless, and accurate, so non-destructive detection is particularly important. Wang et al. [81] used magnetic field scanning imaging to identify small current imbalances within a battery pack to assess the capacity uniformity of the cell within the pack. It can achieve the purpose of accurate battery replacement. Deng et al. [82] developed ultrasound imaging technology as a valuable non-destructive method for characterizing electrolyte status. Its principle is that in the electrode or separator with insufficient wetting,

the ultrasonic attenuation speed is faster than that of the electrode or separator with good wetting. What is more, gas can also block the transmission of ultrasound. Therefore, this technique can be used to study aged cells and find evidence for electrolyte "un-wetting" without disassembling the LIBs. (Figure 6a). In non-destructive testing, the LIB could be considered a black box, which only exports limited information, such as voltage, current, and capacity. By processing voltage and capacity data over the lifetime of a battery, we can use capacity increment (IC) analysis to determine failure information of LIBs [83,84]. Li et al. [85] obtained the change of LIBs material by analyzing the IC curve and comparing it with the standard curve with only testable data. Firstly, at about 3.5V, the peak of NCM811 material is significantly shifted to high potential, which indicates that the cathode material has deteriorated markedly. Besides, a rapid decrease in the reaction peak around 3.7 V was observed. By comparing the reactions of silicon materials, it can be determined that the reaction peak is the Li_4SiO_4 reaction. The more Li_4SiO_4 is produced, the more lithium is consumed irreversibly. Shironita et al. [86] identified the reasons for the capacity degradation of calendar degradation and LIBs after low-temperature cycling through IC curve analysis. There is also a class of non-destructive testing that places the sensor directly in contact with the battery to provide real-time characterization [87]. For example, Peng et al. [88] proposed a new high-precision battery strain sensor method based on a fiber Bragg grating (FBG) sensor, which connected the FBG sensor to the outer surface of the battery for strain monitoring. In addition, the method avoided sensor corrosion and improved reliability while successfully detecting. What is more, many methods have been applied in practice. There are also some recent improvements in 3D imaging, such as X-ray computed tomography (XCT), which allows researchers to look at the microstructure of porous materials with enough resolution to figure out why battery materials fail [89,90]. Taiwo et al. [91] showed microstructure evolution, phase transition, and fracturing of silicon-based electrodes captured by X-ray tomography microscopy during electrochemical lithification. The technology enables the non-destructive real-time study of the degradation and failure process of battery materials. Electrochemical impedance spectroscopy (EIS) is also a very effective battery diagnosis technology and plays a great role in life assessment [92–94]. Teliz et al. [95] presented a method to identify and measure the aging mechanism of commercial 18650 LIBs using EIS technology. They correlated ohm resistance with conductivity losses, SEI layer resistance and charge transfer resistance with lithium-ion losses, and R_w with active material losses, respectively. In addition, the battery impedance reflects valuable electrochemical information about the battery life [96]. Smith et al. [97] showed how to successfully track battery aging using EIS assisted by a microscope. Data from the two methods were connected in an electrochemical finite element model (FEM) to extract variations in inherent battery parameters, such as double-layer capacitance, thin film resistance, exchange current density, and particle radius. Non-destructive testing of battery failure has realized the diagnosis of the failure of battery internal materials through some non-destructive testing parameters or new technical means, which has contributed a lot to the research and use of batteries.

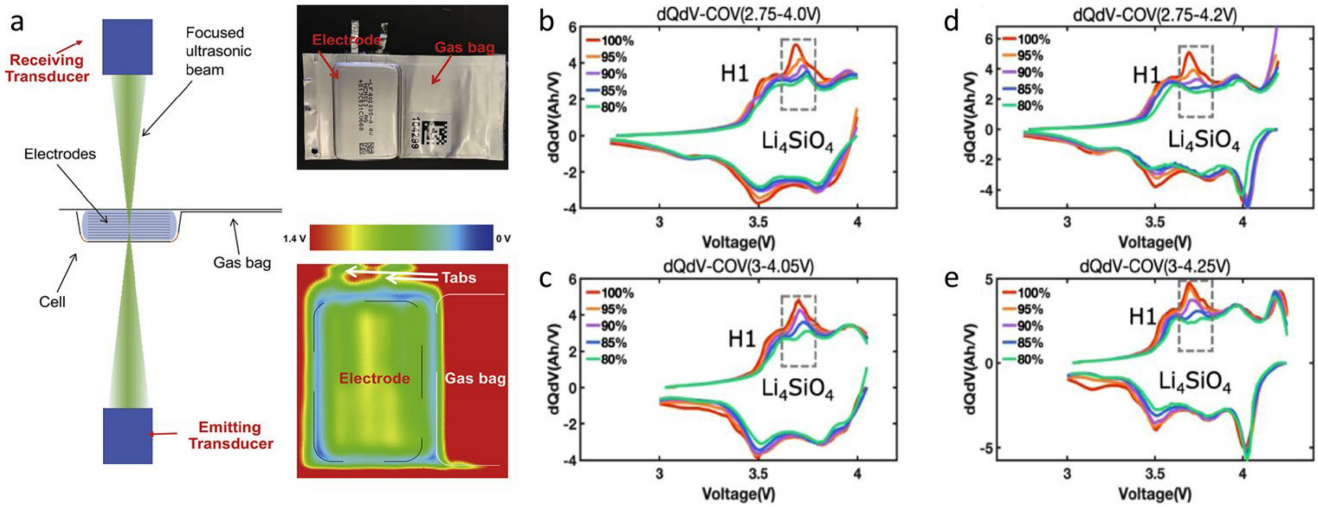

Figure 6. (**a**) Illustration of the principle and structure of the scanning ultrasonic instrument; Reprinted with permission from Ref. [82]. 2020, Elsevier; (**b**–**e**) the incremental capacity analysis of the battery under different life stage. The percenter label in the figure corresponds to cycle of discharge capacity equal to the percenter initial capacity. Reprinted with permission from Ref. [85]. 2018, Elsevier.

8. Methods to Prevent Battery Failure

8.1. Modification of Electrode Structure

The electrochemical failure origin from the side reactions of the material and interface, which will bring capacity degradation and even safety hazards to LIBs. Therefore, the modification of materials will be important research for mitigating failure.

8.2. Modification of Cathode Materials

The modification of cathode materials usually includes ion doping, surface coating, structural design, etc. Ion doping refers to the introduction of other ions into cathode material without changing its original structure, which improves the crystal structure stability of cathode materials [98]. Sun et al. [99] explored the effects of the oxidation states of various dopants (Mg^{2+}, Al^{3+}, Ti^{4+}, Ta^{5+}, and Mo^{6+}) on the electrochemical and structural properties of an Ni-rich cathode material. They doped $Li[Ni_{0.91}Co_{0.09}]O_2$ (NC90) with 1 mol% of Mg^{2+}, Al^{3+}, Ti^{4+}, Ta^{5+}, and Mo^{6+} to obtain cathode materials Mg-NC90, Al-NC90, Ti-NC90, Ta-NC90, and Mo-NC90. The charging and discharging cycles of LIBs showed that the cathode with high oxidation state dopants is significantly more excellent than the undoped cathode. In particular, the LIBs with Ta^{5+} and Mo^{6+} doped NC90 cathodes showed the best performance (Figure 7a,b). Kim et al. [100] doped an appropriate amount of Al to NCM materials, and the newly synthesized materials are superior to NCA and NCM materials with a similar nickel content in cycling and thermal stability. Zhu et al. [101] reduced the charge transfer resistance of LFP through Na doping, increased the diffusion coefficient of lithium, and effectively improved the dynamic performance of LFP. Liu et al. [102] prepared a series of $LiFe_{1-x}Mn_xPO_4/C$ composites by a simple hydrothermal method. The effect of Mn doping on its microstructure and electrochemical properties was studied. The results showed that a small amount of Mn doping can reduce the electrode polarization and electrochemical impedance of the sample, and improve the electrochemical performance. By doping Ti, Sun et al. [103] stabilized the structure of LCO and suppressed the phase transition during the cycle. At a cut-off voltage of 4.5 V, Ti-doped $LiCoO_2$ showed a capacity of 205 mAh g^{-1}. After 200 cycles, the capacity retention rate can reach 97%.

Surface coating is a simple, common, and effective method to improve the properties of battery materials. It involves coating a layer of material on the surface of the battery material; the coating materials investigated to date include carbon, metal oxides, metal car-

bonates, metal aluminates, metal phosphates, metal fluorides, metal oxyfluorides, etc. [104], to prevent contact between the battery's active material and the electrolyte, so that side reactions are decreased [98]. These surface coatings can also improve the wettability of the electrolyte to the electrode, thereby reducing the interfacial charge transfer resistance [105]. There is also a part of the coating that can eliminate corrosive HF and other impurities that bring deterioration to the cathode material [106]. Yang et al. [40] synthesized a more stable single-crystal NCM811 material via the molten-salt route (SC-NCM811@RS). Compared with polycrystalline NCM811 (PC-NCM811), the electrochemical performance and cycle stability of SC-NCM811@RS were significantly improved under the same cycling conditions. Meanwhile, it has better multiplier performance and smaller interfacial charge transfer resistance. (Figure 7c–j). Li et al. [107] compared the TiO_2-coated NCM cathode. It is easy to find that the adverse reactions on the particle surface of the TiO_2 material after coating are inhibited. Moreover, the electrochemical performance and safety at high cut-off voltage are improved (Figure 7k–p). For the coating of LFP materials, mainly coating materials with excellent electrical conductivity, it can not only improve the electrical conductivity of the surface but also inhibit the excessive growth of particles. Yi et al. [108] prepared Ga-coated LFP cathode material. Ga has good electrical conductivity and can rapidly conduct electrons inside LFP cathode material under the synergistic action with C coating, thus improving the electrical conductivity of LFP cathode material. Zhang et al. [26] prepared an all-fluorinated electrolyte, which enabled LCO to form a robust cathode electrolyte interphase (CEI), effectively preventing element dissolution and electrolyte penetration, and protecting the reversible plane sliding along the (003) plane in the cathode of single-crystal $LiCoO_2$. The modification strategies and properties of cathode materials are listed in Table 3.

Table 3. Modification of cathode materials.

Electrode Material	Method of Modification	Performance	Reference
LCO	All-fluorinated electrolyte improving CEI	The fabricated 4.5 V high loading (4 mAh cm^{-2}) $LiCoO_2$ | | graphite full cell delivered an energy density of 430 Wh kg^{-1}, with an excellent capacity retention of 80% after 500 cycles.	[26]
NCM811	Facile molten-salt route	NCM811 material realizes high capacity of 92% after 200 cycles at 0.5 C.	[40]
NC90	Doping with various dopants (Mg^{2+}, Al^{3+}, Ti^{4+}, Ta^{5+}, Mo^{6+})	After doping Ta^{5+} and Mo^{6+} for 3000 cycles at 200 mA g^{-1}, NC90 can still maintain about 81.5% of its initial specific capacity.	[99]
NCM	Doping Al to NCM materials	The capacity of NCMA cathode is 228 mAh g^{-1}, 85% of the initial capacity after 1000 cycles.	[100]
LFP	Doping Na to LFP materials	Na doping increased the diffusion coefficient of LFP ($Li_{1-x}Na_xFePO_4$ (x = 0, 0.05, 0.1, 0.2) 1.21 × 10^{-16}, 1.06 × 10^{-14}, 7.95 × 10^{-15}, and 9.17 × 10^{-15} cm^2 s^{-1}, respectively).	[101]
LFP	Doping Mn to LFP materials	The $LiFe_{0.98}Mn_{0.02}PO_4$/C specific discharge capacity reached 156.0 mAh g^{-1} at a rate of 0.1 C, even at a high rate of 5 C, it can still reach 110.0 mAh g^{-1}.	[102]
LCO	Doping Ti to LCO materials	Ti-doped $LiCoO_2$ exhibits a capacity of 205 mAh g^{-1} at a cut-off voltage of 4.5 V. After 200 cycles, the capacity retention rate is 97%.	[103]
NCM523	TiO_2-coated NCM cathode	The trigger temperature of thermal runaway for the battery using TiO_2-coated NCM523 as cathode material was 257 °C, which was higher than NCM523 cathode (251 °C).	[107]
LFP	Ga-coated LFP cathode	The discharge capacity of 152.6 mAh g^{-1} at 1 C after 100 cycles and a discharge capacity retention rate of 98.77%.	[108]

For the development of ternary material systems, Ni-rich is not the only development, while single crystallization is also an important research direction of various research institutions and battery enterprises. Compared with PC particles, SC particles have unidirectional shrinkage or expansion characteristics, which is a great advantage to reduce crack formation. Therefore, SC materials can improve the stability of materials. Kong et al. [78,109] studied the storage properties and thermal stability of SC-NCM and PC-NCM cathode materials. They found that SC-NCM has better storage performance than PC-NCM materials. It has a lower calorific value and is more stable in the cycle process. This is because the primary particles of SC-NCM materials do not have grain boundaries in the internal structure, which effectively alleviates the formation of microcracks and maintains the integrity of the structure [110–113]. Fan et al. [114] developed the quasi-SC-NCM with primary particles of 3–6 um diameter. The battery they assembled retained 98.7% of its initial capacity after 500 cycles. Dai et al. [31] obtained single-crystal $LiNi_{0.9}Mn_{0.1}O_2$ (SC-NM91), in which the capacity retention reached 85.3% after 300 cycles at 1 C. It was significantly higher than that of PC-NCM (65.8%) (Figure 7q–x). SC-NM91 will not experience surface crushing and cracks after a long cycle, while the structure of PC-NM91 is seriously degraded, leading to microcracks. Meanwhile, the crack will result in a large impedance of PC-NM91 and a serious reduction in cycle stability. For the modification of cathode materials, the pursuit of high energy density and structural stability is the most important task in the modification of cathode materials.

In addition, the development and application of new binders also have a great contribution to the performance improvement of cathode materials. The most commonly used PVDF binder for the positive electrode has some shortcomings such as poor binding affinity, electrical insulation, and high cost [115,116]. For the lithium iron phosphate positive electrode with poor electrical conductivity, Huang et al. [117] designed a new type of water-based lithium ionomer adhesive for lithium-ion batteries. More Li is attached to the molecular chain, increasing the conductivity at the interface between the electrode and the electrolyte. Qiu et al. [118] used cotton as the raw material and synthesized novel functional carboxymethyl cellulose lithium (CMC-Li) material. CMC-Li could increase the content of Li ions in the whole battery, with LIBs exhibiting excellent electrochemical performance. The large structure/volume change and poor conductivity of traditional binders are serious problems. New binders with high concentrations of carboxyl groups can improve electrode stability, and conductive polymers can achieve good conductivity without external conductive agents, which is considered a promising dual-function binder for high-performance lithium-ion batteries [119].

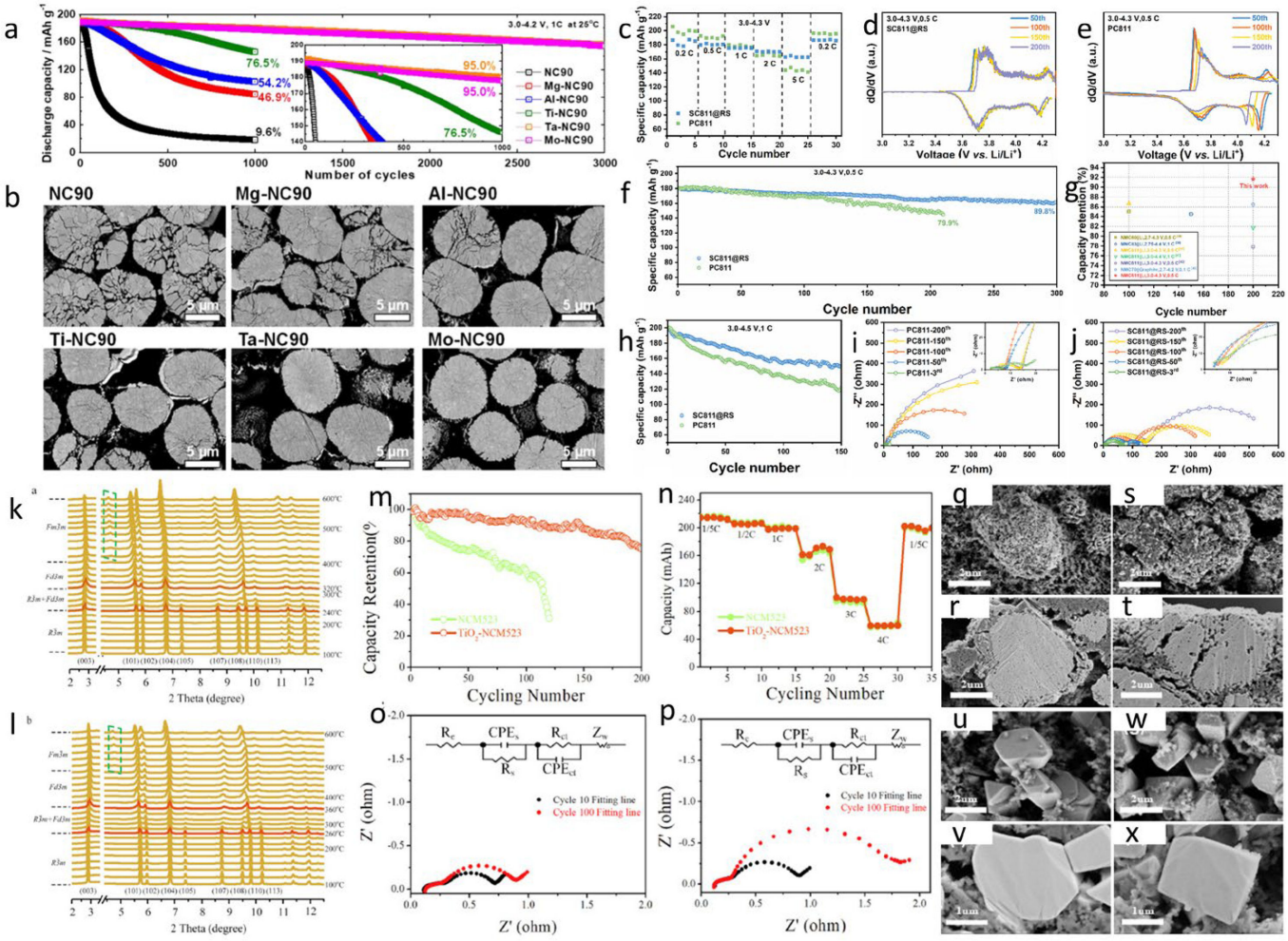

Figure 7. (**a**) Cycling of NC90, Mg-NC90, Al-NC90, Ti-NC90, Ta-NC90, and Mo-NC90 cathodes in pouch-type full cells within the voltage range of 3.0–4.2 V versus graphite at 1 C (200 mA g^{-1}) and 25 °C. (**b**) Cross-sectional images of recovered NC90, Mg-NC90, Al-NC90, Ti-NC90, Ta-NC90, and Mo-NC90 cathodes in the discharged state of 2.7 V after 1000 cycles. Reprinted with permission from Ref. [99]. 2021, Nature; (**c**–**j**) Electrochemical performance comparison of SC-NCM811@RS and PC-NCM811. (**c**) Rate-capability tests of SC-NCM811 and PC-NCM811 electrode. The differential capacity curves of (**d**) SC-NCM811@RS and (**e**) PC-NCM811 in region of 3.0–4.3 V for 200 cycles. Cycling performance at 1C in the voltage region of (**f**) 3.0–4.3 V and (**g**) 3.0–4.5 V. (**h**) The comparison between the Ni-rich cathode batteries and this work in terms of capacity retention and cycle life. The EIS profiles of (**i**) SC-NCM811@RS and (**j**) PC-NCM811 electrode at charging potential Reprinted with permission from Ref. [40]. 2018, Springer; (**k**,**l**) Thermally induced phase transformation of charged (**k**) NCM523 and (**l**) TiO_2-NCM523 cathode materials, (**m**) the cycling of NCM523-and TiO_2-NCM523-based full batteries, (**n**) the rate performances of NCM523 and TiO_2-NCM523-based full batteries, (**o**,**p**) impedance spectrum evolution with an inset image of the equivalent circuit model of (**o**) TiO_2-NCM523 and (**p**) NCM523-based full batteries Reprinted with permission from Ref. [107]. 2018, Elsevier; (**q**–**x**) SEM and cross-section SEM on the cathode side after 200 cycles under 4.5 V of (**q**,**r**) PC-NM91 and (**s**,**t**) SC-NM91 and under 2 C of (**u**,**v**) PC-NM91 and (**w**,**x**) SC-NM91. Reproduced with permission]. Reprinted with permission from Ref. [31]. 2018, ACS Publications.

9. SEI Design and Modification of Anode Materials

In the cycle process of LIBs, SEI is formed in the first turn, so part of the active lithium will be consumed and the capacity will be attenuated to a certain extent [120]. In addition, both silicon cathode with high energy density and commercialized graphite are facing the problem of volume expansion during lithiation and delimitation, SEI of cathode material

surface cannot cope with expansion and contract stresses, this will lead to the cracking of SEI, exposing the active substances to new reaction cross-sections, thus causing the regeneration of SEI. Lithiation and de-lithiation repeatedly result in repeated formation and destruction of the SEI leading to the thickening of the SEI layers [121,122]. What is more, SEI is especially important for the next generation of lithium metal batteries with higher energy density [77]. So many researchers have spent a lot of time on SEI design. Yu et al. [123] used a facile graphite pre-lithiation method by preforming SEI layers on the surface of graphite powders utilizing a specially designed flow cell. The results showed that the initial Coulombic efficiency of $LiFePO_4$ cells increased by 10% (pristine graphite anode cells' initial Coulombic efficiency is 40.4%). This practice, called cathodic pre-lithiation, can greatly compensate for the loss of lithium, thereby increasing the energy density of the cell. In addition to reducing lithium loss, building a stable SEI makes sense. Some additives containing fluorine can also improve SEI formation on anode materials. For example, fluoroethylene carbonate (FEC) additive has been widely used. A lot of research suggests a smoother and more stable SEI layer structure is generated by the introduction of the FEC additive to the electrolyte [48,124]. The various degradation mechanisms observed in high-capacity silicon anode materials are mainly due to expansion/contraction during cycling. Continuous volume changes, as well as particle cracking and comminution, result in the fragmentation of the original SEI film and the formation of new SEI layers on the surface of these broken particles. The SEI reformation is accompanied by electrolyte and lithium-ion depletion, which is particularly problematic for commercial applications given the limited inventory of Li in batteries. Therefore, it is particularly important to build a stable SEI for silicon-containing anode materials [122,125]. Wang et al. [126] constructed a structure of $MoSe_2$-coated Si and used the electrolyte additive FEC to establish SEI. $MoSe_2$ coating can promote the catalytic decomposition of FEC to form a strong and stable SEI, which has high ionic conductivity, and abundant polymerized ethylene carbonate and LiF. Revealing the failure mode of SEI film and guiding high energy density battery to construct stable SEI will play a significant role in accelerating the application of LIBs with higher energy density.

The volume expansion phenomenon in the process of charging and discharging anode materials is the most important material failure problem to be solved [127]. In order to solve the problem of volume expansion, various studies and works have emerged. At present, the resolution of such problems includes material structure (mainly nanostructures and morphological structures) design and new binders. The main type of nanostructured Si that was proposed in the past decades can be classified into 0D (nanoparticles), 1D (nanowires, nanotubes), 2D (thin film), and 3D (porous structure) [128]. Yang et al. [129] demonstrated hollow Si/SiO_x nanosphere/nitrogen-doped carbon superstructure electrodes that are capable of accommodating huge volume changes without pulverization during cycling. Benefiting from the unique double-shelled hollow superstructure, this structure can facilitate the formation of a highly stable SEI layer and provide superior kinetics toward Li-ion storage. The diffusion-controlled process and the capacitance-type reaction can work together to endow the battery with remarkable electrochemical characteristics. Hwang et al. [130] developed an electrospinning technology to produce core–shell fiber electrodes (SiNP@C). In the core–shell fibers, commercially available nanoparticles in the core are wrapped by the carbon shell. The unique core–shell structure resolves various issues of Si anode operations, including pulverization, unstable SEI, and fragile contacts between Si and C. The expansion of electrode material was not much difference after 50 and 500 cycles, and the material showed excellent battery performance of the gravimetric capacity as high as 1384 mAh g^{-1} and cycle life of 300 cycles with almost no capacity loss (Figure 8a–e). An et al. [131] made an ant-nest-like bulk porous silicon structure (AMPSi@C). This structure can prevent silicon anode pulverization and accommodate volume expansion during cycling. The battery cycle performance has been significantly improved: the capacity retention rate was 90% after 1000 cycles, and the expansion rate was 17.8% at the high area capacity of 5.1 mA cm^{-2} (Figure 8g–i).

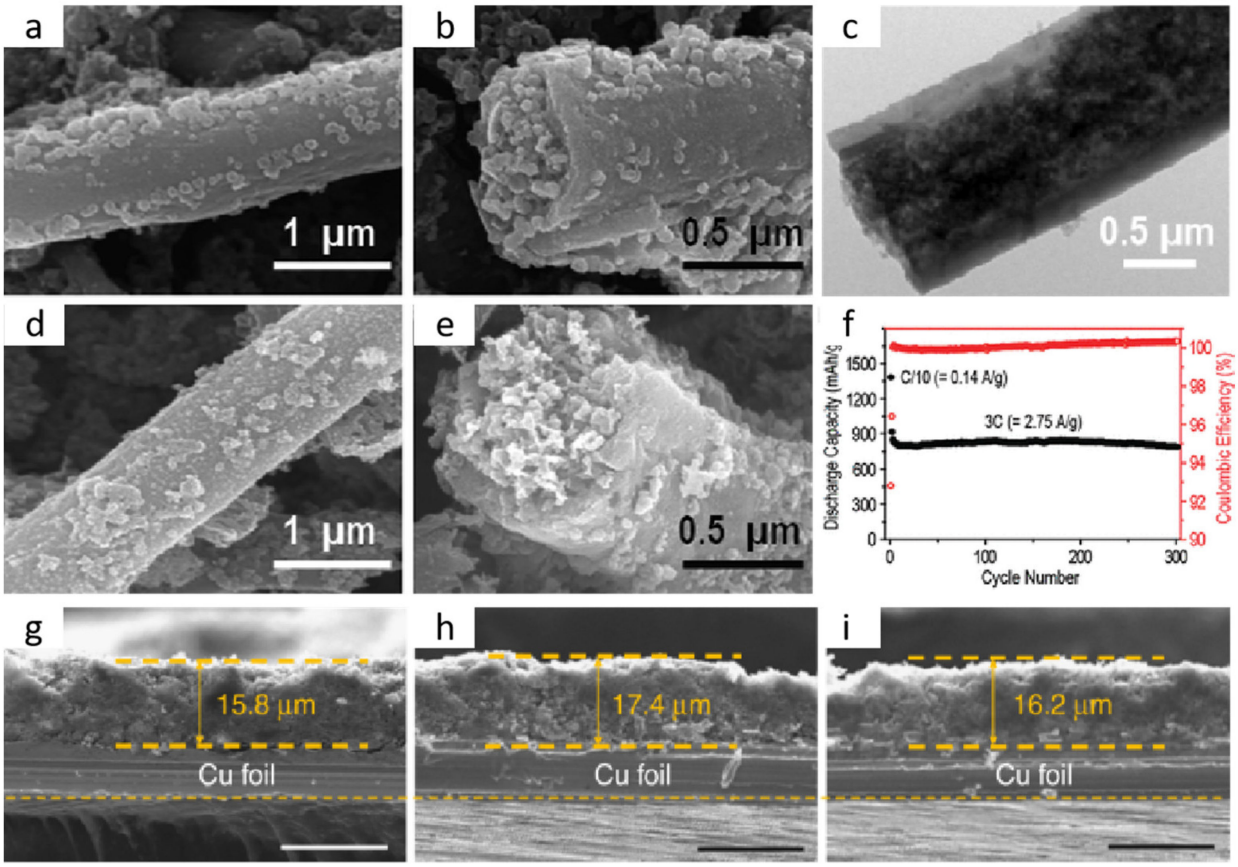

Figure 8. (**a**–**d**) SEM images of SiNP@C after cycling. (**a**,**b**) SEM images of the sidewall and the cross-section of SiNP@C after 50 cycles, (**c**–**e**) SEM images of the sidewall and the cross-section of SiNP@C after 500 cycles, (**f**) cycling performance of SiNP@C measured at 3C rate (2.748 A/g) Reprinted with permission from Ref. [130]. 2012, ACS Publications; electrode swelling measurements of AMPSi@C; (**g**–**i**) cross-sectional SEM images of the AMPSi@C electrode films (**g**) before cycling, (**h**) after full lithiation, and (**i**) de-lithiation, respectively. Reprinted with permission from Ref. [131]. 2019, Nature.

In the research of new binders, we hold the opinion that the ideal electrode binder is expected to have the following capabilities: (1) inherent electronic conductivity under the LIBs environment; (2) mechanical adhesion and ductility with inexhaustible tolerance of large volume change; (3) electrolyte uptake to warrant high ionic conductivity [54]. Wang et al. [132] prepared a porous scaffold of sodium carboxymethyl cellulose using slurry spray technology. As the binder of a silicon anode, the abundant carboxyl group increased the interaction between the binder and Si particles, so that its cyclic stability and rate performance were significantly improved (At 250 mA g^{-1} charge/discharge rate, the battery can retain a capacity of 930 mAh g^{-1} after 85 cycles). Kovalenko et al. [133] reported that an alginate extracted from brown algae can well stabilize the silicon anode. The reversible capacity of silicon in the electrochemical cycle is eight times that of the graphite anode. Su et al. [134] reported a multifunctional polymeric adhesive which consists of a conductive polymer and a stretchable polymer ether thiourea. The multifunctional polymer binder can bend on the surface of nano-silicon particles to form an interwoven continuous 3D network, which is beneficial for electron transfer and mechanical stability. This multifunctional polymer performs superior long-cycle stability (2081 mAh g^{-1} after 300 cycles). There are also some excellent studies [125,135–137] listed in Table 4.

Table 4. Binder to improve battery performance.

Modified Binder	Electrochemical Performance	Reference
Incorporation 5% polyrotaxane to conventional polyacrylic acid binder	Average Coulombic efficiency of 99.92% in the cycle numbers of 2 to 50.	[125]
Sodium carboxymethyl cellulose porous scaffold	At 250 mA g^{-1} charge/discharge rate, the battery can retain capacity of 930 mAh g^{-1} after 85 cycles.	[132]
Mixing Si nanopowder with alginate	At a current density of 4200 mA/g, the reversible Li extraction specific capacity of an alginate-based Si anode is in the range of 1700 to 2000 mAh g^{-1}.	[133]
A multifunctional polymeric binder synthesized by the cross-linking of conducting polymer and poly (ether thioureas).	2081 mAh g^{-1} after 300 cycles and 908 mAh g^{-1} at 8 A g^{-1}.	[134]
Novel conducting polymer based on polyfluorene polymers and introduced carbonyl and methylbenzoic ester	Composite anodes based on this polymer and commercial Si particles exhibit 2100 mAh g^{-1} in Si after 650 cycles without any conductive additive.	[135]
Multifunctional polyaniline hydrogel	83% capacitance retention after 10,000 cycles	[136]
Modified sodium alginate	Without the conductive additives, the resultant batteries have achieved the theoretical specific capacity of $LiFePO_4$ (C/10) and 120 mAh g^{-1} at 1 C for more than 400 cycles.	[137]

10. Optimization of Charging Strategy

With the growing demand for EVs, research and development work of LIBs is now mainly focused on extending the endurance mileage and shortening the charging time. However, on the one hand, fast charging technology will accelerate battery failure and lead to rapid capacity degradation, on the other hand, heat generated during fast charging is often difficult to dissipate quickly, especially in the power battery pack of EVs. It is worth noting that excessive heat generation is more likely to cause safety problems [138]. The new charging strategy is to minimize the anode impact on the battery (such as lithium plating, high temperature, etc.) while shortening the charging time [139,140].

The traditional charging method is mainly constant current (CC) charging, constant voltage (CV) charging. However, there are many new charging strategies that have been proven to save more time, have less heat, or have longer life [138]. The new charging strategies include multistage constant current (MCC) charging strategy, pulse charging strategy, variable current charging strategy, and so on. Using these new charging strategies, it is usually possible to achieve fast charging, reduce heat generation during charging and discharging, avoid Li-plating, and reduce concentration polarization [141–143].

Zhang et al. [144] studied the effect of the charging strategies on the cycle life of a commercial 18650 Li-ion cell using three methods: CC charging, constant power (CP) charging, and MCC charging. It was concluded that the low-rate current is more suitable for the beginning of charging and the end of charging, because the impedance of the battery is larger when the SOC is small, and the high current at the end of charging is prone to Li-plating, which has a great impact on the life of the battery. In addition to changing the charging strategy, the change in ambient temperature during the charging process also has a significant impact on the battery. Yang et al. [145] designed a self-heating structure to preheat the battery to high temperature and then start charging to speed up the transmission

process inside the battery and improve the reaction rate. By limiting the working time of the battery at high temperature to 10 min, the attenuation of the battery material was slowed down, and the capacity of the battery remained 91.7% after 2500 cycles. There is a polarization problem in the battery charging process. What is more, the polarization effect will reduce the power density and cycle stability of the battery [146]. For the polarization problem in the process of battery charging, Li et al. [147] proposed that the pulse charging scheme could reduce the concentration polarization and the charging time, improve the utilization of active materials, and thus produce higher discharge capacity and longer cycle life. For the problem of Li-plating in LIBs at low temperatures, Qin et al. [148] proposed a fast charging strategy without Li-plating, which combines the pulse heating method with the optimal charging method by precisely controlling the battery state (including SOC, temperature, and anodic overpotential). A good power battery fast charging strategy should not only improve the charging speed of the battery, but also not have a bad impact on battery life, and more importantly, ensure safety. Better and more versatile charging strategies deserve further research.

11. Battery Failure Prediction

Electrochemical failure occurring during the life cycle almost cannot be avoided. Moreover, battery safety is usually related to capacity. State of health (SOH) diagnosis and remaining useful life (RUL) prediction can help EVs to monitor battery health in real time and maintain the battery pack before failure [149]. However, the diversity of aging mechanisms of power batteries and the coupling of aging factors, as well as the dynamic operation of batteries in the actual use process, make the accurate life management of power batteries extremely a huge challenge. With the development of computer technology in recent years, a large number of methods for RUL prediction of LIBs have been proposed, which make RUL prediction of batteries more reliable [150].

RUL prediction for the battery can be achieved by both model-based and data-driven approaches [151]. Model-based methods predicting battery RUL are a way based on off-line training data. In the 1990s, the pseudo-two-dimensional(P2D) model was proposed, which accurately described the electrochemical reaction and physical process in LIBs with a series of partial differential equations and algebraic equations, and laid the foundation for the electrochemical mechanism model. This model describes the characteristics of LIBs battery through lithium-ion diffusion in the liquid phase, lithium-ion diffusion in the solid phase, liquid-phase Ohm's law, solid-phase Ohm's law, charge conservation equation, and Butler–Volmer equation [152,153]. In addition, there are equivalent circuit models, fractional order models, and multi-model fusion ideas to achieve more accurate and simple models [154]. Based on the significant physical loss mechanism of a graphite anode, Jin et al. [155] deduced the reduced-order capacitance loss model of the graphite anode. This model captures the two main degradation mechanisms that occur in the graphite anode of LIBs: capacity loss due to SEI layer thickening, and capacity loss due to the production of inactive lithium. The error between the model and the experimental results of capacity degradation is within 20%. The numerical simulation method has been able to accurately simulate the electrochemical reaction in the LIBs. The form of multi-physical field coupling gives more possibilities to numerically simulate the battery life decay under working conditions. Although this numerical simulation model can achieve the full life cycle output of battery internal parameters, it is a huge challenge to build a multi-dimensional and high-precision model, which includes not only the detailed acquisition of battery parameters but also the coupling relationship between parameters [156].

Thanks to the development of computer technology, the algorithm applied to machine learning has been verified, making machine learning once again lead the boom. The non-linear attenuation of battery capacity makes capacity prediction a challenge. Data-driven machine learning can solve this problem well. The content of the data-driven prediction method is data mining, practice, and promotion based on the capacity decay curve. For example, use raw input signals (current, voltage) for training. Moreover, preprocessed

features from voltage, current, impedance, or power curves also can be input to machine learning models for training. Machine learning does not need a comprehensive understanding of the mechanism of power batteries and electrochemical, and has the great advantages of simple process and small computation [157]. Machine learning (ML) methods include supervised learning and unsupervised learning to deal with regression, classification, clustering, and other problems. Among ML methods, adaptive state estimation methods, such as the particle filter (PF) algorithm and Kalman filter (KF) method, have been frequently utilized for battery SOH and RUL prediction [158]. Wang et al. [159] conducted accelerated cycle life studies on commercial LIBs. The influence of test parameters (time, temperature, depth of discharge) was studied in depth. The life model was used to describe the effect of temperature and service time on battery capacity fade. Wu et al. [160] defined RUL by analyzing the voltage curve of the battery terminal under different cycles in the charging process. In addition, they used a feedforward neural network (FNN) to simulate the relationship between RUL and the charge curve, which proved that the method was simple and effective. Considering the nonlinear characteristics of the LIBs charging curve, the importance sampling (IS) method is employed for FNN input. On this basis, an online RUL estimation method according to FNN and IS are proposed. Finally, experiments and numerical comparisons are conducted to validate the proposed method. However, unlike LIBs that maintain a constant operating state in the laboratory, in the real world, the operating state may change throughout the battery life cycle. EVs' batteries experience temperature differences that include seasonality, inter-battery variations within the battery pack, and a constantly changing SOC window related to travel distance, and depending on driving conditions, the charge and discharge current/power levels can influence battery degradation [157,161] Song et al. [162] proposed a kind of real data of EVs based on a big data platform, and constructed an intelligent SOH estimation framework. This method extracts health features from historical operation data, and then implements deep learning in a feedforward neural network driven by degradation index. The effectiveness of the proposed method was verified by monitoring 700 vehicles with different driving modes for one year. The results showed that the proposed framework can effectively estimate SOH with a maximum relative error of 4.5%. RUL prediction is an important part of BMS. The RUL prediction function in BMS can play a great role in battery life and safety management. Accurate prediction can completely avoid failure by removing, isolating, or replacing batteries that enter the predicted risk area, thereby mitigating the hazard without sacrificing the system performance that typically accompanies alternative safety materials and safety equipment [163]. The development of more accurate and less computational models is an important direction of LIBs management, which is the key to improving the performance of EVs.

12. Summary and Prospect

This paper systematically analyzed the mechanism of LIBs electrochemical failure and summarized the detection methods of battery failure, failure prediction, and protection methods. Based on the change of the bulk phase, surface, and interface of the material, combined with the characteristics of the side reaction that occurred in the porous electrode and the characterization methods, the failure mechanism was described in detail. According to the electrochemical reaction foundation and material science, the response methods to battery failure, including materials, cells, and battery management system (BMS), are fully analyzed. In addition, we also introduced the main methods of battery failure prediction in detail to achieve a comprehensive understanding of battery failure.

In our view, battery failure is inevitable, which can only be slowed down. In order to achieve this goal, the optimization of the material is essential, containing active material and electrolyte. However, the development of new materials cannot be solved overnight. Therefore, better performance of batteries during their actual use depends on the excellent monitoring and prediction capabilities of the BMS.

In a word, to alleviate the electrochemical failure of LIBs, we need to focus on battery materials, battery design, life prediction, and management systems. The best option is to maintain battery capacity while improving battery safety.

Author Contributions: W.L. wrote the paper; H.L., Z.H., W.J., J.Z. (Jing Zeng), X.L. and Y.Z. designed the structures of the paper; P.Z. and J.Z. (Jinbao Zhao) reviewed the paper. All authors have read and agreed to the published version of the manuscript.

Funding: This research was funded by National Natural Science Foundation of China (21875195), the Key Project of Science and Technology of Xiamen (3502Z20201013), the Fundamental Research Funds for the Central Universities (20720190040), Yunnan Major Scientific and Technological Projects (202202AG050003).

Data Availability Statement: Not applicable.

Conflicts of Interest: The authors declare no conflict of interest.

References

1. Yu, X.; Manthiram, A. Sustainable Battery Materials for Next-Generation Electrical Energy Storage. *Adv. Energy Sustain. Res.* **2021**, *2*, 2000102. [CrossRef]
2. Xie, J.; Lu, Y. A retrospective on lithium-ion batteries. *Nat. Commun.* **2020**, *11*, 2499. [CrossRef] [PubMed]
3. Li, H.; Kong, X.; Liu, C.; Zhao, J. Study on thermal stability of nickel-rich/silicon-graphite large capacity lithium ion battery. *Appl. Therm. Eng.* **2019**, *161*, 114144. [CrossRef]
4. Liu, W.; Oh, P.; Liu, X.; Lee, M.-J.; Cho, W.; Chae, S.; Kim, Y.; Cho, J. Nickel-Rich Layered Lithium Transition-Metal Oxide for High-Energy Lithium-Ion Batteries. *Angew. Chem. Int. Ed.* **2015**, *54*, 4440–4457. [CrossRef] [PubMed]
5. Miao, Y.; Hynan, P.; von Jouanne, A.; Yokochi, A. Current Li-Ion Battery Technologies in Electric Vehicles and Opportunities for Advancements. *Energies* **2019**, *12*, 1074. [CrossRef]
6. Deng, J.; Bae, C.; Denlinger, A.; Miller, T. Electric Vehicles Batteries: Requirements and Challenges. *Joule* **2020**, *4*, 511–515. [CrossRef]
7. Hannan, M.A.; Hoque, M.M.; Mohamed, A.; Ayob, A. Review of energy storage systems for electric vehicle applications: Issues and challenges. *Renew. Sustain. Energy Rev.* **2017**, *69*, 771–789. [CrossRef]
8. Goodenough, J.B.; Kim, Y. Challenges for Rechargeable Li Batteries. *Chem. Mater.* **2010**, *22*, 587–603. [CrossRef]
9. Krupp, A.; Beckmann, R.; Diekmann, T.; Ferg, E.; Schuldt, F.; Agert, C. Calendar aging model for lithium-ion batteries considering the influence of cell characterization. *J. Energy Storage* **2022**, *45*, 103506. [CrossRef]
10. Eduardo, R.; Pascal, V.; Pelissier, S. Calendar and cycling ageing combination of batteries in electric vehicles. *Microelectron. Reliab.* **2018**, *88–90*, 1212–1215.
11. Maik, N.; Michael, S.; Peter, K.; Holger, C.H.; Andreas, J. Analysis and modeling of calendar aging of a commercial $LiFePO_4$/graphite cell. *J. Energy Storage* **2018**, *17*, 153–169.
12. Ren, D.; Hsu, H.; Li, R.; Feng, X.; Guo, D.; Han, X.; Lu, L.; He, X.; Gao, S.; Hou, J.; et al. A comparative investigation of aging effects on thermal runaway behavior of lithium-ion batteries. *eTransportation* **2019**, *2*, 100034. [CrossRef]
13. Han, X.; Lu, L.; Zheng, Y.; Feng, X.; Li, Z.; Li, J.; Ouyang, M. A review on the key issues of the lithium ion battery degradation among the whole life cycle. *eTransportation* **2019**, *1*, 100005. [CrossRef]
14. Fleischhammer, M.; Waldmann, T.; Bisle, G.; Hogg, B.-I.; Wohlfahrt-Mehrens, M. Interaction of cyclic ageing at high-rate and low temperatures and safety in lithium-ion batteries. *J. Power Sources* **2015**, *274*, 432–439. [CrossRef]
15. Kim, K.M.; Ly, N.V.; Won, J.H.; Lee, Y.-G.; Cho, W.I.; Ko, J.M.; Kaner, R.B. Improvement of lithium-ion battery performance at low temperature by adopting polydimethylsiloxane-based electrolyte additives. *Electrochim. Acta* **2014**, *136*, 182–188. [CrossRef]
16. Mussa, A.S.; Liivat, A.; Marzano, F.; Klett, M.; Philippe, B.; Tengstedt, C.; Lindbergh, G.; Edström, K.; Lindström, R.W.; Svens, P. Fast-charging effects on ageing for energy-optimized automotive $LiNi_{1/3}Mn_{1/3}Co_{1/3}O_2$/graphite prismatic lithium-ion cells. *J. Power Sources* **2019**, *422*, 175–184. [CrossRef]
17. Vetter, J.; Novák, P.; Wagner, M.R.; Veit, C.; Möller, K.-C.; Besenhard, J.O.; Winter, M.; Wohlfahrt-Mehrens, M.; Vogler, C.; Hammouche, A. Ageing mechanisms in lithium-ion batteries. *J. Power Sources* **2005**, *147*, 269–281. [CrossRef]
18. Käbitz, S.; Gerschler, J.B.; Ecker, M.; Yurdagel, Y.; Emmermacher, B.; André, D.; Mitsch, T.; Sauer, D.U. Cycle and calendar life study of a graphite | $LiNi_{1/3}Mn_{1/3}Co_{1/3}O_2$ Li-ion high energy system. Part A: Full cell characterization. *J. Power Sources* **2013**, *239*, 572–583. [CrossRef]
19. Zheng, J.; Gu, M.; Xiao, J.; Zuo, P.; Wang, C.; Zhang, J.-G. Corrosion/Fragmentation of Layered Composite Cathode and Related Capacity/Voltage Fading during Cycling Process. *Nano Lett.* **2013**, *13*, 3824–3830. [CrossRef]
20. He, Y.; Jiang, L.; Chen, T.; Xu, Y.; Jia, H.; Yi, R.; Xue, D.; Song, M.; Genc, A.; Bouchet-Marquis, C.; et al. Progressive growth of the solid–electrolyte interphase towards the Si anode interior causes capacity fading. *Nat. Nanotechnol.* **2012**, *16*, 10. [CrossRef]
21. Atalay, S.; Sheikh, M.; Mariani, A.; Merla, Y.; Bower, E.; Widanage, W.D. Theory of battery ageing in a lithium-ion battery: Capacity fade, nonlinear ageing and lifetime prediction. *J. Power Sources* **2020**, *478*, 229026. [CrossRef]

22. Han, X.; Ouyang, M.; Lu, L.; Li, J.; Zheng, Y.; Li, Z. A comparative study of commercial lithium ion battery cycle life in electrical vehicle: Aging mechanism identification. *J. Power Sources* **2014**, *251*, 38–54. [CrossRef]
23. He, W.; Guo, W.; Wu, H.; Lin, L.; Liu, Q.; Han, X.; Xie, Q.; Liu, P.; Zheng, H.; Wang, L.; et al. Challenges and Recent Advances in High Capacity Li-Rich Cathode Materials for High Energy Density Lithium-Ion Batteries. *Adv. Mater.* **2021**, *33*, 2005937. [CrossRef] [PubMed]
24. Lyu, Y.; Wu, X.; Wang, K.; Feng, Z.; Cheng, T.; Liu, Y.; Wang, M.; Chen, R.; Xu, L.; Zhou, J.; et al. An Overview on the Advances of $LiCoO_2$ Cathodes for Lithium-Ion Batteries. *Adv. Energy Mater.* **2021**, *11*, 2000982. [CrossRef]
25. Zhang, J.-C.; Liu, Z.-D.; Zeng, C.-H.; Luo, J.-W.; Deng, Y.-D.; Cui, X.-Y.; Chen, Y.-N. High-voltage $LiCoO_2$ cathodes for high-energy-density lithium-ion battery. *Rare Met.* **2022**, *41*, 3946–3956. [CrossRef]
26. Zhang, J.; Wang, P.; Bai, P.; Wan, H.; Liu, S.; Hou, S.; Pu, X.; Xia, J.; Zhang, W.; Wang, Z.; et al. Interfacial Design for a 4.6 V High-Voltage Single-Crystalline $LiCoO_2$ Cathode. *Adv. Mater.* **2022**, *34*, 2108353. [CrossRef]
27. Li, L.; Wu, L.; Wu, F.; Song, S.; Zhang, X.; Fu, C.; Yuan, D.; Xiang, Y. Review—Recent Research Progress in Surface Modification of $LiFePO_4$ Cathode Materials. *J. Electrochem. Soc.* **2017**, *164*, A2138. [CrossRef]
28. Chen, S.-P.; Lv, D.; Chen, J.; Zhang, Y.-H.; Shi, F.-N. Review on Defects and Modification Methods of $LiFePO_4$ Cathode Material for Lithium-Ion Batteries. *Energy Fuels* **2022**, *36*, 1232–1251. [CrossRef]
29. Li, Z.; Yang, J.; Guang, T.; Fan, B.; Zhu, K.; Wang, X. Controlled Hydrothermal/Solvothermal Synthesis of High-Performance $LiFePO_4$ for Li-Ion Batteries. *Small Methods* **2021**, *5*, 2100193. [CrossRef]
30. Nitta, N.; Wu, F.; Lee, J.T.; Yushin, G. Li-ion battery materials: Present and future. *Mater. Today* **2015**, *18*, 252–264. [CrossRef]
31. Dai, P.; Kong, X.; Yang, H.; Li, J.; Zeng, J.; Zhao, J. Single-Crystal Ni-Rich Layered $LiNi_{0.9}Mn_{0.1}O_2$ Enables Superior Performance of Co-Free Cathodes for Lithium-Ion Batteries. *ACS Sustain. Chem. Eng.* **2022**, *10*, 4381–4390. [CrossRef]
32. Li, J.; Wang, X.; Kong, X.; Yang, H.; Zeng, J.; Zhao, J. Insight into the Kinetic Degradation of Stored Nickel-Rich Layered Cathode Materials for Lithium-Ion Batteries. *ACS Sustain. Chem. Eng.* **2021**, *9*, 10547–10556. [CrossRef]
33. Chen, X.; Li, S.; Hu, Y.; Chai, Y.; Li, D.; Zuo, W.; Zhang, Z.; Yang, Y. Failure mechanism of $Li_{1+x}(NCM)_{1-x}O_2$ layered oxide cathode material during capacity degradation. *Energy Storage Sci. Technol.* **2019**, *8*, 1003. [CrossRef]
34. Xia, Y.; Zheng, J.; Wang, C.; Gu, M. Designing principle for Ni-rich cathode materials with high energy density for practical applications. *Nano Energy* **2018**, *49*, 434–452. [CrossRef]
35. Yan, P.; Zheng, J.; Lv, D.; Wei, Y.; Zheng, J.; Wang, Z.; Kuppan, S.; Yu, J.; Luo, L.; Edwards, D.; et al. Atomic-Resolution Visualization of Distinctive Chemical Mixing Behavior of Ni, Co, and Mn with Li in Layered Lithium Transition-Metal Oxide Cathode Materials. *Chem. Mater.* **2015**, *27*, 5393–5401. [CrossRef]
36. Sun, H.; Zhao, K. Electronic Structure and Comparative Properties of $LiNixMnyCozO_2$ Cathode Materials. *J. Phys. Chem. C* **2017**, *121*, 6002–6010. [CrossRef]
37. Lin, Q.; Guan, W.; Meng, J.; Huang, W.; Wei, X.; Zeng, Y.; Li, J.; Zhang, Z. A new insight into continuous performance decay mechanism of Ni-rich layered oxide cathode for high energy lithium ion batteries. *Nano Energy* **2018**, *54*, 313–321. [CrossRef]
38. Jung, S.-K.; Gwon, H.; Hong, J.; Park, K.-Y.; Seo, D.-H.; Kim, H.; Hyun, J.; Yang, W.; Kang, K. Understanding the Degradation Mechanisms of $LiNi_{0.5}Co_{0.2}Mn_{0.3}O_2$ Cathode Material in Lithium Ion Batteries. *Adv. Energy Mater.* **2014**, *4*, 1300787. [CrossRef]
39. Noh, H.-J.; Youn, S.; Yoon, C.S.; Sun, Y.-K. Comparison of the structural and electrochemical properties of layered $Li[Ni_xCo_yMn_z]O_2$ (x = 1/3, 0.5, 0.6, 0.7, 0.8 and 0.85) cathode material for lithium-ion batteries. *J. Power Sources* **2013**, *233*, 121–130. [CrossRef]
40. Yang, H.; Kong, X.; Li, J.; Dai, P.; Zeng, J.; Yang, Y.; Zhao, J. In-situ construction of a thermodynamically stabilized interface on the surface of single crystalline Ni-rich cathode materials via a one-step molten-salt route. *Nano Res.* **2022**, *6*, 1–9. [CrossRef]
41. Li, D.; Li, H.; Danilov, D.L.; Gao, L.; Chen, X.; Zhang, Z.; Zhou, J.; Eichel, R.-A.; Yang, Y.; Notten, P.H. Degradation mechanisms of $C_6/LiNi_{0.5}Mn_{0.3}Co_{0.2}O_2$ Li-ion batteries unraveled by non-destructive and post-mortem methods. *J. Power Sources* **2019**, *416*, 163–174. [CrossRef]
42. Liu, X.; Ren, D.; Hsu, H.; Feng, X.; Xu, G.-L.; Zhuang, M.; Gao, H.; Lu, L.; Han, X.; Chu, Z.; et al. Thermal Runaway of Lithium-Ion Batteries without Internal Short Circuit. *Joule* **2018**, *2*, 2047–2064. [CrossRef]
43. Hou, J.; Feng, X.; Wang, L.; Liu, X.; Ohma, A.; Lu, L.; Ren, D.; Huang, W.; Li, Y.; Yi, M.; et al. Unlocking the self-supported thermal runaway of high-energy lithium-ion batteries. *Energy Storage Mater.* **2021**, *39*, 395–402. [CrossRef]
44. Zhang, H.; Yang, Y.; Ren, D.; Wang, L.; He, X. Graphite as anode materials: Fundamental mechanism, recent progress and advances. *Energy Storage Mater.* **2021**, *36*, 147–170. [CrossRef]
45. Andersen, H.L.; Djuandhi, L.; Mittal, U.; Sharma, N. Strategies for the Analysis of Graphite Electrode Function. *Adv. Energy Mater.* **2021**, *11*, 2102693. [CrossRef]
46. Cui, Q.; Zhong, Y.; Pan, L.; Zhang, H.; Yang, Y.; Liu, D.; Teng, F.; Bando, Y.; Yao, J.; Wang, X. Recent Advances in Designing High-Capacity Anode Nanomaterials for Li-Ion Batteries and Their Atomic-Scale Storage Mechanism Studies. *Adv. Sci.* **2018**, *5*, 1700902. [CrossRef] [PubMed]
47. Zhu, H.; Russell, J.A.; Fang, Z.; Barnes, P.; Li, L.; Efaw, C.; Muenzer, A.; May, J.; Hamal, K.; Cheng, I.F.; et al. A Comparison of Solid Electrolyte Interphase Formation and Evolution on Highly Oriented Pyrolytic and Disordered Graphite Negative Electrodes in Lithium-Ion Batteries. *Small* **2021**, *17*, 2105292. [CrossRef]
48. An, S.J.; Li, J.; Daniel, C.; Mohanty, D.; Nagpure, S.; Wood, D.L. The state of understanding of the lithium-ion-battery graphite solid electrolyte interphase (SEI) and its relationship to formation cycling. *Carbon* **2016**, *105*, 52–76. [CrossRef]

49. Peled, E.; Menkin, S. Review—SEI: Past, Present and Future. *J. Electrochem. Soc.* **2017**, *164*, A1703. [CrossRef]
50. Yoshio, M.; Tsumura, T.; Dimov, N. Electrochemical behaviors of silicon based anode material. *J. Power Sources* **2005**, *146*, 10–14. [CrossRef]
51. Pidaparthy, S.; Luo, M.; Rodrigues, M.-T.F.; Zuo, J.-M.; Abraham, D.P. Physicochemical Heterogeneity in Silicon Anodes from Cycled Lithium-Ion Cells. *ACS Appl. Mater. Interfaces* **2022**, *14*, 38660–38668. [CrossRef]
52. Xiao, Q.; Gu, M.; Yang, H.; Li, B.; Zhang, C.; Liu, Y.; Liu, F.; Dai, F.; Yang, L.; Liu, Z.; et al. Inward lithium-ion breathing of hierarchically porous silicon anodes. *Nat. Commun.* **2015**, *6*, 8844. [CrossRef]
53. Wu, H.; Cui, Y. Designing nanostructured Si anodes for high energy lithium ion batteries. *Nano Today* **2012**, *7*, 414–429. [CrossRef]
54. Wu, M.; Xiao, X.; Vukmirovic, N.; Xun, S.; Das, P.K.; Song, X.; Olalde-Velasco, P.; Wang, D.; Weber, A.Z.; Wang, L.-W.; et al. Toward an Ideal Polymer Binder Design for High-Capacity Battery Anodes. *J. Am. Chem. Soc.* **2013**, *135*, 12048–12056. [CrossRef]
55. Ko, M.; Chae, S.; Cho, J. Challenges in Accommodating Volume Change of Si Anodes for Li-Ion Batteries. *ChemElectroChem* **2015**, *2*, 1645–1651. [CrossRef]
56. Wetjen, M.; Solchenbach, S.; Pritzl, D.; Hou, J.; Tileli, V.; Gasteiger, H.A. Morphological Changes of Silicon Nanoparticles and the Influence of Cutoff Potentials in Silicon-Graphite Electrodes. *J. Electrochem. Soc.* **2018**, *165*, A1503. [CrossRef]
57. McDowell, M.T.; Ryu, I.; Lee, S.W.; Wang, C.; Nix, W.D.; Cui, Y. Studying the Kinetics of Crystalline Silicon Nanoparticle Lithiation with In Situ Transmission Electron Microscopy. *Adv. Mater.* **2012**, *24*, 6034–6041. [CrossRef]
58. Zhang, H.; Yang, Y.; Xu, H.; Wang, L.; Lu, X.; He, X. $Li_4Ti_5O_{12}$ spinel anode: Fundamentals and advances in rechargeable batteries. *InfoMat* **2022**, *4*, e12228. [CrossRef]
59. Yuan, T.; Tan, Z.; Ma, C.; Yang, J.; Ma, Z.-F.; Zheng, S. Challenges of Spinel $Li_4Ti_5O_{12}$ for Lithium-Ion Battery Industrial Applications. *Adv. Energy Mater.* **2017**, *7*, 1601625. [CrossRef]
60. Chen, Z.; Belharouak, I.; Sun, Y.-K.; Amine, K. $Li_4Ti_5O_{12}$ for High-Power, Long-Life, and Safe Lithium-Ion Batteries. In *Lithium Batteries*; John Wiley & Sons, Ltd.: Hoboken, NJ, USA, 2013; pp. 277–290. [CrossRef]
61. Ghosh, A.; Ghamouss, F. Role of Electrolytes in the Stability and Safety of Lithium Titanate-Based Batteries. *Front. Mater.* **2020**, *7*, 186. [CrossRef]
62. He, Y.-B.; Li, B.; Liu, M.; Zhang, C.; Lv, W.; Yang, C.; Li, J.; Du, H.; Zhang, B.; Yang, Q.-H.; et al. Gassing in $Li_4Ti_5O_{12}$-based batteries and its remedy. *Sci. Rep.* **2012**, *2*, 913. [CrossRef] [PubMed]
63. Wang, G.; Aubin, M.; Mehta, A.; Tian, H.; Chang, J.; Kushima, A.; Sohn, Y.; Yang, Y. Stabilization of Sn Anode through Structural Reconstruction of a Cu–Sn Intermetallic Coating Layer. *Adv. Mater.* **2020**, *32*, 2003684. [CrossRef] [PubMed]
64. Derrien, G.; Hassoun, J.; Panero, S.; Scrosati, B. Nanostructured Sn–C Composite as an Advanced Anode Material in High-Performance Lithium-Ion Batteries. *Adv. Mater.* **2007**, *19*, 2336–2340. [CrossRef]
65. Ying, H.; Han, W.-Q. Metallic Sn-Based Anode Materials: Application in High-Performance Lithium-Ion and Sodium-Ion Batteries. *Adv. Sci.* **2017**, *4*, 1700298. [CrossRef] [PubMed]
66. Zinth, V.; von Lüders, C.; Hofmann, M.; Hattendorff, J.; Buchberger, I.; Erhard, S.; Rebelo-Kornmeier, J.; Jossen, A.; Gilles, R. Lithium plating in lithium-ion batteries at sub-ambient temperatures investigated by in situ neutron diffraction. *J. Power Sources* **2014**, *271*, 152–159. [CrossRef]
67. Gao, T.; Han, Y.; Fraggedakis, D.; Das, S.; Zhou, T.; Yeh, C.-N.; Xu, S.; Chueh, W.C.; Li, J.; Bazant, M.Z. Interplay of Lithium Intercalation and Plating on a Single Graphite Particle. *Joule* **2021**, *5*, 393–414. [CrossRef]
68. Li, Z.; Huang, J.; Liaw, B.Y.; Metzler, V.; Zhang, J. A review of lithium deposition in lithium-ion and lithium metal secondary batteries. *J. Power Sources* **2014**, *254*, 168–182. [CrossRef]
69. Mei, W.; Jiang, L.; Liang, C.; Sun, J.; Wang, Q. Understanding of Li-plating on graphite electrode: Detection, quantification and mechanism revelation. *Energy Storage Mater.* **2021**, *41*, 209–221. [CrossRef]
70. Zhang, S.S.; Xu, K.; Jow, T.R. Study of the charging process of a $LiCoO_2$-based Li-ion battery. *J. Power Sources* **2006**, *160*, 1349–1354. [CrossRef]
71. Li, H.; Ji, W.; Zhang, P.; Zhao, J. Safety boundary of power battery based on quantitative lithium deposition. *J. Energy Storage* **2022**, *52*, 104789. [CrossRef]
72. Sarkar, A.; Shrotriya, P.; Nlebedim, I.C. Anodic Interfacial Evolution in Extremely Fast Charged Lithium-Ion Batteries. *ACS Appl. Energy Mater.* **2022**, *5*, 3179–3188. [CrossRef]
73. Ho, A.S.; Parkinson, D.Y.; Finegan, D.P.; Trask, S.E.; Jansen, A.N.; Tong, W.; Balsara, N.P. 3D Detection of Lithiation and Lithium Plating in Graphite Anodes during Fast Charging. *ACS Nano* **2021**, *15*, 10480–10487. [CrossRef]
74. Petzl, M.; Kasper, M.; Danzer, M.A. Lithium plating in a commercial lithium-ion battery—A low-temperature aging study. *J. Power Sources* **2015**, *275*, 799–807. [CrossRef]
75. Li, Y.; Feng, X.; Ren, D.; Ouyang, M.; Lu, L.; Han, X. Thermal Runaway Triggered by Plated Lithium on the Anode after Fast Charging. *ACS Appl. Mater. Interfaces* **2019**, *11*, 46839–46850. [CrossRef]
76. Sreenarayanan, B.; Tan, D.H.S.; Bai, S.; Li, W.; Bao, W.; Meng, Y.S. Quantification of lithium inventory loss in micro silicon anode via titration-gas chromatography. *J. Power Sources* **2022**, *531*, 231327. [CrossRef]
77. Li, H.; Wen, Z.; Wu, D.; Ji, W.; He, Z.; Wang, F.; Yang, Y.; Zhang, P.; Zhao, J. Achieving a Stable Solid Electrolyte Interphase and Enhanced Thermal Stability by a Dual-Functional Electrolyte Additive toward a High-Loading $LiNi_{0.8}Mn_{0.1}Co_{0.1}O_2$/Lithium Pouch Battery. *ACS Appl. Mater. Interfaces* **2021**, *13*, 57142–57152. [CrossRef]

78. Kong, X.; Zhang, Y.; Li, J.; Yang, H.; Dai, P.; Zeng, J.; Zhao, J. Single-crystal structure helps enhance the thermal performance of Ni-rich layered cathode materials for lithium-ion batteries. *Chem. Eng. J.* **2022**, *434*, 134638. [CrossRef]
79. Zhang, X.; Gao, Y.; Guo, B.; Zhu, C.; Zhou, X.; Wang, L.; Cao, J. A novel quantitative electrochemical aging model considering side reactions for lithium-ion batteries. *Electrochim. Acta* **2020**, *343*, 136070. [CrossRef]
80. Yang, X.-G.; Liu, T.; Gao, Y.; Ge, S.; Leng, Y.; Wang, D.; Wang, C.-Y. Asymmetric Temperature Modulation for Extreme Fast Charging of Lithium-Ion Batteries. *Joule* **2019**, *3*, 3002–3019. [CrossRef]
81. Wang, H.; Dai, L.; Mao, L.; Liu, Y.; Jin, Y.; Wu, Q. In Situ Detection of Lithium-Ion Battery Pack Capacity Inconsistency Using Magnetic Field Scanning Imaging. *Small Methods* **2019**, *6*, 2101358. [CrossRef]
82. Deng, Z.; Huang, Z.; Shen, Y.; Huang, Y.; Ding, H.; Luscombe, A.; Johnson, M.; Harlow, J.E.; Gauthier, R.; Dahn, J.R. Ultrasonic Scanning to Observe Wetting and "Unwetting" in Li-Ion Pouch Cells. *Joule* **2020**, *4*, 2017–2029. [CrossRef]
83. Zhang, S.S. Problems and their origins of Ni-rich layered oxide cathode materials. *Energy Storage Mater.* **2020**, *24*, 247–254. [CrossRef]
84. Ryu, H.H.; Park, K.J.; Yoon, C.S.; Sun, Y.K. Capacity Fading of Ni-Rich $Li[Ni_xCo_yMn_{1-x-y}]O_2$ ($0.6 \leq x \leq 0.95$) Cathodes for High-Energy-Density Lithium-Ion Batteries: Bulk or Surface Degradation? *Chem. Mater.* **2018**, *3*, 1155–1163. [CrossRef]
85. Li, H.; Ji, W.; He, Z.; Zhang, Y.; Zhao, J. Distinct capacity fade modes of Nickel-rich/Graphite-SiO_x power lithium ion battery. *J. Energy Storage* **2022**, *47*, 103830. [CrossRef]
86. Mendoza-Hernandez, O.S.; Hosono, E.; Asakura, D.; Matsuda, H.; Shironita, S.; Umeda, M.; Sone, Y. Impact of Calendar Degradation on the Performance of $LiFePO_4$—Graphite Li-Ion Cells during Charge-Discharge Cycling at −5 °C. *J. Electrochem. Soc.* **2019**, *166*, A3525. [CrossRef]
87. Mouravieff, C. Unlocking cell chemistry evolution with operando fibre optic infrared spectroscopy in commercial Na(Li)-ion batteries. *Nature Energy* **2022**. [CrossRef]
88. Peng, J.; Zhou, X.; Jia, S.; Jin, Y.; Xu, S.; Chen, J. High precision strain monitoring for lithium ion batteries based on fiber Bragg grating sensors. *J. Power Sources* **2019**, *433*, 226692. [CrossRef]
89. Scharf, J.; Chouchane, M.; Finegan, D.P.; Lu, B.; Redquest, C.; Kim, M.-C.; Yao, W.; Franco, A.A.; Gostovic, D.; Liu, Z.; et al. Bridging nano- and microscale X-ray tomography for battery research by leveraging artificial intelligence. *Nat. Nanotechnol.* **2022**, *17*, 446–459. [CrossRef]
90. Gayon-Lombardo, A.; Mosser, L.; Brandon, N.P.; Cooper, S.J. Pores for thought: Generative adversarial networks for stochastic reconstruction of 3D multi-phase electrode microstructures with periodic boundaries. *NPJ Comput. Mater.* **2020**, *6*, 82. [CrossRef]
91. Taiwo, O.O.; Paz-García, J.M.; Hall, S.A.; Heenan, T.M.; Finegan, D.P.; Mokso, R.; Villanueva-Pérez, P.; Patera, A.; Brett, D.J.; Shearing, P.R. Microstructural degradation of silicon electrodes during lithiation observed via operando X-ray tomographic imaging. *J. Power Sources* **2017**, *342*, 904–912. [CrossRef]
92. Pastor-Fernández, C.; Uddin, K.; Chouchelamane, G.H.; Widanage, W.D.; Marco, J. A Comparison between Electrochemical Impedance Spectroscopy and Incremental Capacity-Differential Voltage as Li-ion Diagnostic Techniques to Identify and Quantify the Effects of Degradation Modes within Battery Management Systems. *J. Power Sources* **2017**, *360*, 301–318. [CrossRef]
93. Gordon, I.J.; Genies, S.; Larbi, G.S.; Boulineau, A.; Daniel, L.; Alias, M. Original implementation of Electrochemical Impedance Spectroscopy (EIS) in symmetric cells: Evaluation of post-mortem protocols applied to characterize electrode materials for Li-ion batteries. *J. Power Sources* **2016**, *307*, 788–795. [CrossRef]
94. Gaberšček, M. Understanding Li-Based Battery Materials Via Electrochemical Impedance Spectroscopy. *Nat. Commun.* **2021**, *12*, 6513. [CrossRef]
95. Teliz, E.; Zinola, C.F.; Díaz, V. Identification and quantification of ageing mechanisms in Li-ion batteries by Electrochemical impedance spectroscopy. *Electrochim. Acta* **2022**, *426*, 140801. [CrossRef]
96. Jiang, B.; Zhu, J.; Wang, X.; Wei, X.; Shang, W.; Dai, H. A comparative study of different features extracted from electrochemical impedance spectroscopy in state of health estimation for lithium-ion batteries. *Appl. Energy* **2022**, *322*, 119502. [CrossRef]
97. R-Smith, N.A.-Z.; Leitner, M.; Alic, I.; Toth, D.; Kasper, M.; Romio, M.; Surace, Y.; Jahn, M.; Kienberger, F.; Ebner, A.; et al. Assessment of lithium ion battery ageing by combined impedance spectroscopy, functional microscopy and finite element modelling. *J. Power Sources* **2021**, *512*, 230459. [CrossRef]
98. Zhang, H.; Zhang, J. An overview of modification strategies to improve $LiNi_{0.8}Co_{0.1}Mn_{0.1}O_2$ (NCM811) cathode performance for automotive lithium-ion batteries. *eTransportation* **2021**, *7*, 100105. [CrossRef]
99. Sun, H.H.; Kim, U.-H.; Park, J.-H.; Park, S.-W.; Seo, D.-H.; Heller, A.; Mullins, C.B.; Yoon, C.S.; Sun, Y.-K. Transition metal-doped Ni-rich layered cathode materials for durable Li-ion batteries. *Nat. Commun.* **2021**, *12*, 6552. [CrossRef]
100. Kim, U.-H.; Kuo, L.-Y.; Kaghazchi, P.; Yoon, C.S.; Sun, Y.-K. Quaternary Layered Ni-Rich NCMA Cathode for Lithium-Ion Batteries. *ACS Energy Lett.* **2019**, *4*, 576–582. [CrossRef]
101. Zhu, Y.-R.; Zhang, R.; Deng, L.; Yi, T.-F.; Ye, M.-F.; Yao, J.-H.; Dai, C.-S. Lithium-Ion Insertion Kinetics of Na-Doped $LiFePO_4$ as Cathode Materials for Lithium-Ion Batteries. *Metall. Mater. Trans. E* **2015**, *2*, 33–38. [CrossRef]
102. Liu, Y.; Gu, Y.-J.; Deng, J.-L.; Luo, G.-Y.; Wu, F.-Z.; Mai, Y.; Dai, X.-Y.; Li, J.-Q. Effect of doped Mn on improving the electrochemical performance of $LiFePO_4$. *J. Mater. Sci. Mater. Electron.* **2020**, *31*, 2887–2894. [CrossRef]
103. Sun, L.; Zhang, Z.; Hu, X.; Tian, H.; Zhang, Y.; Yang, X. Realization of Ti Doping by Electrostatic Assembly to Improve the Stability of $LiCoO_2$ Cycled to 4.5 V. *J. Electrochem. Soc.* **2019**, *166*, A1793. [CrossRef]

104. Chen, Z.; Qin, Y.; Amine, K.; Sun, Y.-K. Role of surface coating on cathode materials for lithium-ion batteries. *J. Mater. Chem.* **2010**, *20*, 7606–7612. [CrossRef]
105. Nisar, U.; Muralidharan, N.; Essehli, R.; Amin, R.; Belharouak, I. Valuation of Surface Coatings in High-Energy Density Lithium-ion Battery Cathode Materials. *Energy Storage Mater.* **2021**, *38*, 309–328. [CrossRef]
106. Hall, D.S.; Gauthier, R.B.; Eldesoky, A.; Murray, V.S.; Dahn, J.R. New Chemical Insights into the Beneficial Role of Al_2O_3 Cathode Coatings in Lithium-ion Cells. *ACS Appl. Mater. Interfaces* **2019**, *11*, 14095–14100. [CrossRef]
107. Li, Y.; Liu, X.; Ren, D.; Hsu, H.; Xu, G.-L.; Hou, J.; Wang, L.; Feng, X.; Lu, L.; Xu, W.; et al. Toward a high-voltage fast-charging pouch cell with TiO_2 cathode coating and enhanced battery safety. *Nano Energy* **2020**, *71*, 104643. [CrossRef]
108. Yi, D.; Cui, X.; Li, N.; Zhang, L.; Yang, D. Enhancement of Electrochemical Performance of $LiFePO_4$@C by Ga Coating. *ACS Omega* **2020**, *5*, 9752–9758. [CrossRef]
109. Kong, X.; Zhang, Y.; Peng, S.; Zeng, J.; Zhao, J. Superiority of Single-Crystal to Polycrystalline $LiNi_xCo_yMn_{1-x-y}O_2$ Cathode Materials in Storage Behaviors for Lithium-Ion Batteries. *ACS Sustain. Chem. Eng.* **2020**, *8*, 14938–14948. [CrossRef]
110. Guo, Q.; Huang, J.; Liang, Z.; Potapenko, H.; Zhou, M.; Tang, X.; Zhong, S. The use of a single-crystal nickel-rich layered NCM cathode for excellent cycle performance of lithium-ion batteries. *New J. Chem.* **2021**, *45*, 3652–3659. [CrossRef]
111. Li, F.; Kong, L.; Sun, Y.; Jin, Y.; Hou, P. Micron-sized monocrystalline $LiNi_{1/3}Co_{1/3}Mn_{1/3}O_2$ as high-volumetric-energy-density cathode for lithium-ion batteries. *J. Mater. Chem. A* **2018**, *6*, 12344–12352. [CrossRef]
112. Guo, J.; Li, W. Synthesis of Single-Crystal $LiNi_{0.7}Co_{0.15}Mn_{0.15}O_2$ Materials for Li-Ion Batteries by a Sol–Gel Method. *ACS Appl. Energy Mater.* **2022**, *5*, 397–406. [CrossRef]
113. Klein, S.; Bärmann, P.; Fromm, O.; Borzutzki, K.; Reiter, J.; Fan, Q.; Winter, M.; Placke, T.; Kasnatscheew, J. Prospects and limitations of single-crystal cathode materials to overcome cross-talk phenomena in high-voltage lithium ion cells. *J. Mater. Chem. A* **2021**, *9*, 7546–7555. [CrossRef]
114. Fan, X.; Liu, Y.; Ou, X.; Zhang, J.; Zhang, B.; Wang, D.; Hu, G. Unravelling the influence of quasi single-crystalline architecture on high-voltage and thermal stability of $LiNi_{0.5}Co_{0.2}Mn_{0.3}O_2$ cathode for lithium-ion batteries. *Chem. Eng. J.* **2020**, *393*, 124709. [CrossRef]
115. Huang, S.; Huang, X.; Huang, Y.; He, X.; Zhuo, H.; Chen, S. Rational Design of Effective Binders for $LiFePO_4$ Cathodes. *Polymers* **2021**, *13*, 3146. [CrossRef]
116. Cholewinski, A.; Si, P.; Uceda, M.; Pope, M.; Zhao, B. Polymer Binders: Characterization and Development toward Aqueous Electrode Fabrication for Sustainability. *Polymers* **2021**, *13*, 631. [CrossRef]
117. Huang, S.; Shao, Z.; Wang, D.; Wang, W.; Wang, F.; Wang, J. Enhanced Electrochemical Properties of $LiFePO_4$ Cathode Using Waterborne Lithiated Ionomer Binder in Li-Ion Batteries with Low Amount. *ACS Sustain. Chem. Eng.* **2018**, *6*, 12650–12657. [CrossRef]
118. Qiu, L.; Shao, Z.; Wang, D.; Wang, F.; Wang, W.; Wang, J. Carboxymethyl cellulose lithium (CMC-Li) as a novel binder and its electrochemical performance in lithium-ion batteries. *Cellulose* **2014**, *21*, 2789–2796. [CrossRef]
119. Shi, Y.; Zhou, X.; Yu, G. Material and Structural Design of Novel Binder Systems for High-Energy, High-Power Lithium-Ion Batteries. *Acc. Chem. Res.* **2017**, *50*, 2642–2652. [CrossRef]
120. Xin, C.; Gao, J.; Luo, R.; Zhou, W. Prelithiation Reagents and Strategies on High Energy Lithium-Ion Batteries. *Chem. Eur. J.* **2022**, *28*, e202104282. [CrossRef]
121. Heiskanen, S.K.; Kim, J.; Lucht, B.L. Generation and Evolution of the Solid Electrolyte Interphase of Lithium-Ion Batteries. *Joule* **2019**, *3*, 2322–2333. [CrossRef]
122. Prado, A.Y.R.; Rodrigues, M.-T.F.; Trask, S.E.; Shaw, L.; Abraham, D.P. Electrochemical Dilatometry of Si-Bearing Electrodes: Dimensional Changes and Experiment Design. *J. Electrochem. Soc.* **2020**, *167*, 160551. [CrossRef]
123. Yu, Y.; Yang, Z.; Liu, Y.; Xie, J. Achieving SEI preformed graphite in flow cell to mitigate initial lithium loss. *Carbon* **2022**, *196*, 589–595. [CrossRef]
124. Choi, N.-S.; Yew, K.H.; Lee, K.Y.; Sung, M.; Kim, H.; Kim, S.-S. Effect of fluoroethylene carbonate additive on interfacial properties of silicon thin-film electrode. *J. Power Sources* **2006**, *161*, 1254–1259. [CrossRef]
125. Choi, S.; Kwon, T.-W.; Coskun, A.; Choi, J.W. Highly elastic binders integrating polyrotaxanes for silicon microparticle anodes in lithium ion batteries. *Science* **2017**, *357*, 279–283. [CrossRef] [PubMed]
126. Wang, J.; Yang, Z.; Mao, B.; Wang, Y.; Jiang, Y.; Cao, M. Transgenic Engineering on Silicon Surfaces Enables Robust Interface Chemistry. *ACS Energy Lett.* **2022**, *7*, 2781–2791. [CrossRef]
127. Liu, N.; Lu, Z.; Zhao, J.; McDowell, M.T.; Lee, H.-W.; Zhao, W.; Cui, Y. A pomegranate-inspired nanoscale design for large-volume-change lithium battery anodes. *Nat. Nanotechnol.* **2014**, *9*, 187–192. [CrossRef]
128. Li, H.; Li, H.; Lai, Y.; Yang, Z.; Yang, Q.; Liu, Y.; Zheng, Z.; Liu, Y.; Sun, Y.; Zhong, B.; et al. Revisiting the Preparation Progress of Nano-Structured Si Anodes toward Industrial Application from the Perspective of Cost and Scalability. *Adv. Energy Mater.* **2022**, *12*, 2102181. [CrossRef]
129. Yang, C.; Zhang, Y.; Zhou, J.; Lin, C.; Lv, F.; Wang, K.; Feng, J.; Xu, Z.; Li, J.; Guo, S. Hollow Si/SiO_x nanosphere/nitrogen-doped carbon superstructure with a double shell and void for high-rate and long-life lithium-ion storage. *J. Mater. Chem. A* **2018**, *6*, 8039–8046. [CrossRef]
130. Hwang, T.H.; Lee, Y.M.; Kong, B.-S.; Seo, J.-S.; Choi, J.W. Electrospun Core–Shell Fibers for Robust Silicon Nanoparticle-Based Lithium Ion Battery Anodes. *Nano Lett.* **2012**, *12*, 802–807. [CrossRef]

131. An, W.; Gao, B.; Mei, S.; Xiang, B.; Fu, J.; Wang, L.; Zhang, Q.; Chu, P.K.; Huo, K. Scalable synthesis of ant-nest-like bulk porous silicon for high-performance lithium-ion battery anodes. *Nat. Commun.* **2019**, *10*, 1447. [CrossRef]
132. Guo, J.; Wang, C. A polymer scaffold binder structure for high capacity silicon anode of lithium-ion battery. *Chem. Commun.* **2010**, *46*, 1428–1430. [CrossRef]
133. Kovalenko, I.; Zdyrko, B.; Magasinski, A.; Hertzberg, B.; Milicev, Z.; Burtovyy, R.; Luzinov, I.; Yushin, G. A Major Constituent of Brown Algae for Use in High-Capacity Li-Ion Batteries. *Science* **2011**, *334*, 75–79. [CrossRef]
134. Su, Y.; Feng, X.; Zheng, R.; Lv, Y.; Wang, Z.; Zhao, Y.; Shi, L.; Yuan, S. Binary Network of Conductive Elastic Polymer Constraining Nanosilicon for a High-Performance Lithium-Ion Battery. *ACS Nano* **2021**, *15*, 14570–14579. [CrossRef]
135. Liu, G.; Xun, S.; Vukmirovic, N.; Song, X.; Olalde-Velasco, P.; Zheng, H.; Battaglia, V.S.; Wang, L.; Yang, W. Polymers with Tailored Electronic Structure for High Capacity Lithium Battery Electrodes. *Adv. Mater.* **2011**, *23*, 4679–4683. [CrossRef]
136. Pan, L.; Yu, G.; Zhai, D.; Lee, H.R.; Zhao, W.; Liu, N.; Wang, H.; Tee, B.C.K.; Shi, Y.; Cui, Y.; et al. Hierarchical nanostructured conducting polymer hydrogel with high electrochemical activity. *Proc. Natl. Acad. Sci. USA* **2012**, *109*, 9287–9292. [CrossRef]
137. Ling, M.; Qiu, J.; Li, S.; Yan, C.; Kiefel, M.J.; Liu, G.; Zhang, S. Multifunctional SA-PProDOT Binder for Lithium Ion Batteries. *Nano Lett.* **2015**, *15*, 4440–4447. [CrossRef]
138. Tomaszewska, A.; Chu, Z.; Feng, X.; O'Kane, S.; Liu, X.; Chen, J.; Ji, C.; Endler, E.; Li, R.; Liu, L.; et al. Lithium-ion battery fast charging: A review. *eTransportation* **2019**, *1*, 100011. [CrossRef]
139. Trentadue, G.; Lucas, A.; Otura, M.; Pliakostathis, K.; Zanni, M.; Scholz, H. Evaluation of Fast Charging Efficiency under Extreme Temperatures. *Energies* **2018**, *11*, 1937. [CrossRef]
140. Chen, C.; Shang, F.; Salameh, M.; Krishnamurthy, M. Challenges and Advancements in Fast Charging Solutions for EVs: A Technological Review. In Proceedings of the 2018 IEEE Transportation Electrification Conference and Expo (ITEC), Long Beach, CA, USA, 13–14 June 2018; pp. 695–701. [CrossRef]
141. Waldmann, T.; Kasper, M.; Wohlfahrt-Mehrens, M. Optimization of Charging Strategy by Prevention of Lithium Deposition on Anodes in high-energy Lithium-ion Batteries—Electrochemical Experiments. *Electrochim. Acta* **2015**, *178*, 525–532. [CrossRef]
142. Anseán, D.; Dubarry, M.; Devie, A.; Liaw, B.; García, V.; Viera, J.; González, M. Fast charging technique for high power $LiFePO_4$ batteries: A mechanistic analysis of aging. *J. Power Sources* **2016**, *321*, 201–209. [CrossRef]
143. Abdel-Monem, M.; Trad, K.; Omar, N.; Hegazy, O.; van den Bossche, P.; van Mierlo, J. Influence analysis of static and dynamic fast-charging current profiles on ageing performance of commercial lithium-ion batteries. *Energy* **2017**, *120*, 179–191. [CrossRef]
144. Zhang, S.S. The effect of the charging protocol on the cycle life of a Li-ion battery. *J. Power Sources* **2006**, *161*, 1385–1391. [CrossRef]
145. Yang, X.-G.; Vishnugopi, B.S.; Mukherjee, P.P.; Wang, W.; Sun, F.; Wang, C.-Y. Advancements in extreme fast charging to foster sustainable electrification. *One Earth* **2022**, *5*, 216–219. [CrossRef]
146. Zheng, J.; Lu, J.; Amine, K.; Pan, F. Depolarization effect to enhance the performance of lithium ions batteries. *Nano Energy* **2017**, *33*, 497–507. [CrossRef]
147. Li, J.; Murphy, E.; Winnick, J.; Kohl, P.A. The effects of pulse charging on cycling characteristics of commercial lithium-ion batteries. *J. Power Sources* **2001**, *102*, 302–309. [CrossRef]
148. Qin, Y.; Zuo, P.; Chen, X.; Yuan, W.; Huang, R.; Yang, X.; Du, J.; Lu, L.; Han, X.; Ouyang, M. An ultra-fast charging strategy for lithium-ion battery at low temperature without lithium plating. *J. Energy Chem.* **2022**, *72*, 442–452. [CrossRef]
149. Reis, M.S.; Jiang, B. Predicting the lifetime of Lithium–Ion batteries: Integrated feature extraction and modeling through sequential Unsupervised-Supervised Projections (USP). *Chem. Eng. Sci.* **2022**, *252*, 117510. [CrossRef]
150. Zhang, J.; Lee, J. A review on prognostics and health monitoring of Li-ion battery. *J. Power Sources* **2011**, *196*, 6007–6014. [CrossRef]
151. Zhang, Y.; Xiong, R.; He, H.; Qu, X.; Pecht, M. Aging characteristics-based health diagnosis and remaining useful life prognostics for lithium-ion batteries. *eTransportation* **2019**, *1*, 100004. [CrossRef]
152. Doyle, M.; Fuller, T.F.; Newman, J. Modeling of Galvanostatic Charge and Discharge of the Lithium/Polymer/Insertion Cell. *J. Electrochem. Soc.* **1993**, *140*, 1526. [CrossRef]
153. Xiong, R.; Li, L.; Li, Z.; Yu, Q.; Mu, H. An electrochemical model based degradation state identification method of Lithium-ion battery for all-climate electric vehicles application. *Appl. Energy* **2018**, *219*, 264–275. [CrossRef]
154. Lin, C.; Mu, H.; Xiong, R.; Cao, J. Multi-Model Probabilities Based State Fusion Estimation Method of Lithium-Ion Battery for Electric Vehicles: State-of-energy—ScienceDirect. Available online: https://www.sciencedirect.com/science/article/pii/S0306261916306626 (accessed on 24 November 2022).
155. Jin, X.; Vora, A.; Hoshing, V.; Saha, T.; Shaver, G.; García, R.E.; Wasynczuk, O.; Varigonda, S. Physically-based reduced-order capacity loss model for graphite anodes in Li-ion battery cells. *J. Power Sources* **2017**, *342*, 750–761. [CrossRef]
156. Su, X.; Wang, S.; Pecht, M.; Zhao, L.; Ye, Z. Interacting multiple model particle filter for prognostics of lithium-ion batteries. *Microelectron. Reliab.* **2017**, *70*, 59–69. [CrossRef]
157. Sulzer, V.; Mohtat, P.; Aitio, A.; Lee, S.; Yeh, Y.T.; Steinbacher, F.; Khan, M.U.; Lee, J.W.; Siegel, J.B.; Stefanopoulou, A.G.; et al. The challenge and opportunity of battery lifetime prediction from field data. *Joule* **2021**, *5*, 1934–1955. [CrossRef]
158. Yang, D.; Zhang, X.; Pan, R.; Wang, Y.; Chen, Z. A novel Gaussian process regression model for state-of-health estimation of lithium-ion battery using charging curve. *J. Power Sources* **2018**, *384*, 387–395. [CrossRef]
159. Wang, J.; Liu, P.; Hicks-Garner, J.; Sherman, E.; Soukiazian, S.; Verbrugge, M.; Tataria, H.; Musser, J.; Finamore, P. Cycle-life model for graphite-$LiFePO_4$ cells. *J. Power Sources* **2011**, *196*, 3942–3948. [CrossRef]

160. Wu, J.; Zhang, C.; Chen, Z. An online method for lithium-ion battery remaining useful life estimation using importance sampling and neural networks. *Appl. Energy* **2016**, *173*, 134–140. [CrossRef]
161. Su, L.; Zhang, J.; Huang, J.; Ge, H.; Li, Z.; Xie, F.; Liaw, B.Y. Path dependence of lithium ion cells aging under storage conditions. *J. Power Sources* **2016**, *315*, 35–46. [CrossRef]
162. Song, L.; Zhang, K.; Liang, T.; Han, X.; Zhang, Y. Intelligent state of health estimation for lithium-ion battery pack based on big data analysis. *J. Energy Storage* **2020**, *32*, 101836. [CrossRef]
163. Finegan, D.P.; Cooper, S.J. Battery Safety: Data-Driven Prediction of Failure. *Joule* **2019**, *3*, 2599–2601. [CrossRef]